Geophysical Journal International

Geophys. J. Int. (2014) **199,** 880–893
GJI Seismology

doi: 10.1093/gji/ggu269

Seismic wave propagation in fully anisotropic axisymmetric media

Martin van Driel[1] and Tarje Nissen-Meyer[2]

[1]*Institute of Geophysics, ETH Zurich, Sonneggstrasse 5, 8092 Zurich, Switzerland, E-mail: Martin@vanDriel.de*
[2]*Department of Earth Sciences, University of Oxford, South Parks Road, Oxford, OX1 3AN, United Kingdom*

Accepted 2014 July 11. Received 2014 July 9; in original form 2014 February 3

SUMMARY

We present a numerical method to compute 3-D elastic waves in fully anisotropic axisymmetric media. This method is based on a decomposition of the wave equation into a series of uncoupled 2-D equations for which the dependence of the wavefield on the azimuth can be solved analytically. Four independent equations up to quadrupole order appear as solutions for moment-tensor sources located on the symmetry axis while single forces can be accommodated by two separate solutions up to dipole order. This decomposition gives rise to an efficient solution of the 3-D wave equation in a 2-D axisymmetric medium. First, we prove the validity of the decomposition of the wavefield in the presence of general anisotropy. Then we use it to derive the reduced 2-D equations of motions and discretize them using the spectral element method. Finally, we benchmark the numerical implementation for global wave propagation at 1 Hz and consider inner core anisotropy as an application for high-frequency wave propagation in anisotropic media at frequencies up to 2 Hz.

Key words: Seismic anisotropy; Computational seismology; Theoretical seismology; Wave propagation.

1 INTRODUCTION

Seismic anisotropy describes directional dependence of seismic wave speeds and occurs in the Earth for various reasons: most importantly, mantle flow tends to align intrinsically anisotropic crystals causing lattice-preferred orientation which is expected to account for the bulk of the upper mantle anisotropy (Long & Becker 2010). Secondly, anisotropy can be caused by preferential alignment of small scale heterogeneities, called shape-preferred orientation: 3-D structure of purely isotropic material on a subwavelength scale can cause apparent anisotropy, which was realized for layered media by Backus (1962) and is used for computational benefits using homogenization techniques to upscale earth models (e.g. Guillot *et al.* 2010).

Anisotropy is globally observed in the upper mantle, where different velocities for horizontally and vertically polarized shear waves are needed to explain observed Love and Rayleigh wave speeds. The upper mantle of the 1-D earth model PREM (Dziewonski & Anderson 1981) has radial anisotropy while ak135 (Kennett *et al.* 1995) is isotropic. Wang *et al.* (2013) analyse whether the anisotropy in 1-D models is due to intrinsic anisotropy or can be explained by fine layering. The study by Auer *et al.* (2013) is the most recent example of a tomographic model for shear wave anisotropy on a whole mantle scale and compares various anisotropic models (Kustowski *et al.* 2008; Panning *et al.* 2010) to identify regions in which the anisotropic models have reached a certain maturity. Also, structures above the core–mantle boundary (CMB) such as ultra low velocity zones (ULVZ) and large low shear velocity provinces (LLSVP) are expected to be anisotropic (e.g. Panning & Romanowicz 2004; Long 2009; Nowacki *et al.* 2011; Walker *et al.* 2011; Cottaar & Romanowicz 2013). In the inner core, hexagonal anisotropy with a fast axis in north–south direction is observed both with normal modes (Deuss *et al.* 2010) and inner core body waves (Irving & Deuss 2011).

To capture these diverse appearances of seismic anisotropy across the scales, full waveform modelling is needed, preferably up to high resolution (1–2 Hz) as observed in waveforms for lowermost mantle and inner-core anisotropy. While anisotropy is included in many numerical wave propagation solvers (e.g. Igel *et al.* 1995; Komatitsch *et al.* 2000; de la Puente *et al.* 2007; Moczo *et al.* 2007), full 3-D wave propagation is not feasible for the observed body wave frequencies on the global scale due to its tremendous cost in solving for up to 10^{12} degrees of freedom at these resolutions. In a series of papers, Nissen-Meyer *et al.* (2007a,b, 2008) developed a novel approach to global seismic wave propagation that is based on a decomposition of the 3-D wave equation into a series of uncoupled 2-D equations that is valid for axisymmetric models. The axisymmetric approach has three major advantages over full 3-D methods: (1) it enables the storage of the wavefields that provide the basis for computing Fréchet sensitivity kernels (Dahlen *et al.* 2000), which is not feasible with full 3-D methods due to disk space requirements; (2) it allows the inclusion 2.5-D lateral heterogeneities that are effectively modelled as ringlike structures around the symmetry axis giving rise to various applications in a high-frequency

approximation that are not tractable with 1-D methods and (3) it is computationally several orders of magnitude less expensive than full 3-D methods and hence allows the simulation of higher frequencies. Axisymmetric approaches have been presented earlier using finite difference (Alterman & Karal 1968; Igel & Weber 1995, 1996; Chaljub & Tarantola 1997; Thomas *et al.* 2000; Takenaka *et al.* 2003; Toyokuni *et al.* 2005) or pseudospectral methods (Furumura *et al.* 1998), but most of these studies assume azimuthally symmetric sources (monopoles) and hence cannot model arbitrary earthquake sources, but rather resemble explosive sources or a certain geometry for strike slip events (Jahnke *et al.* 2008). More recently, Toyokuni & Takenaka (2006, 2012) generalized their method to include moment tensor sources, attenuation and the Earth centre. Furthermore, these methods are all based on isotropic media and especially the finite difference methods have to deal with large dispersion errors for interface sensitive waves like surface waves and diffracted waves. Here we generalize the spectral element method by Nissen-Meyer *et al.* (2007a) to fully anisotropic axisymmetric media to overcome these issues. This in combination with (2) and (3) above enables the simulation of high-frequency body waves in anisotropic structures such as the D$''$ and the inner core in a 2.5-D approximation.

The numerical implementation (*AxiSEM*) was recently published under GNU general public license (`www.axisem.info`) and a whole variety of applications is presented by Nissen-Meyer *et al.* (2014). Stähler *et al.* (2012) use this method to compute finite frequency sensitivity kernels for triplicated *P* waves, which is inaccurate with other methods such as the one by Dahlen *et al.* (2000) due to the strong influence of the upper-mantle discontinuities in comparison to their sensitivity to mantle heterogeneity. Colombi *et al.* (2012, 2013) compute boundary topography kernels, analyse the sensitivity of different phases in comparison to there sensitivity to mantel heterogeneity and invert for CMB topography. Boué *et al.* (2013) use *AxiSEM* to compute synthetic reference seismograms to interpret noise correlations.

This paper is structured as follows: in the first section, we discuss analytically that the decomposition of the elastic wave equation into a multipole series remains valid in the presence of general anisotropy by means of two arguments based on normal mode coupling and commuting operators. In the second section we apply this decomposition to derive the 2-D weak form of the reduced wave equations and discretize them spatially based on a spectral element method (SEM). In the third section, we benchmark the new implementation at high (1 Hz) and low frequency (normal modes observed at frequencies of a few mHz) against reference solutions and find excellent agreement. In the last section, we apply our method to inner-core anisotropy at 2 Hz as an example of the anisotropic parameter regime covered by *AxiSEM*. Comprehensive appendices list the full discretized stiffness terms for the multipole expansion explicitly.

2 MULTIPOLE EXPANSION

For clarity and generality, we outline two different approaches which show that the decomposition into a multipole series remains valid and still results in a series of uncoupled equations in the presence of general anisotropy: The first one takes a normal mode perspective and generalizes the argument by Nissen-Meyer *et al.* (2007a) that is valid for spherically symmetric non-rotating elastic isotropic (SNREI) earth models by expressing the wavefield in the normal mode basis and anlysing the mode coupling selection rules. The second approach is more abstract and general as it is based on two essential properties of the physical system under consideration: invariance under rotation and linearity, thereby dropping the necessity for a spherical domain and including a variety of other equations.

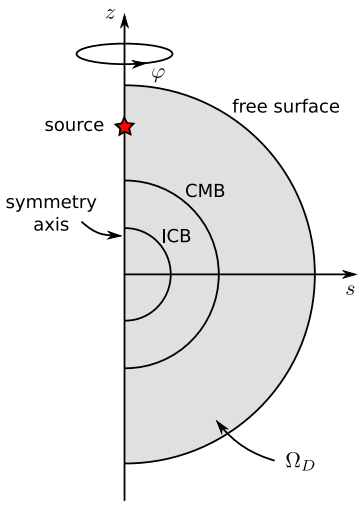

Figure 1. The cylindrical coordinate system (s, φ, z) and the reduced semi-circular 2-D domain Ω_D for global wave propagation in axisymmetric media.

2.1 Statement of the problem

In the cylindrical coordinate system (s, φ, z), any square integrable function $\mathbf{u}$ defined on a domain Ω symmetric with respect to the polar axis $\hat{\mathbf{e}}_z$ (Fig. 1) can be decomposed by applying a Fourier transform in the angular coordinate φ as

$$\mathbf{u}(s,z,\varphi) = \sum_{m=-\infty}^{\infty} \underbrace{\left[u_s^m(s,z)\hat{\mathbf{e}}_s(\varphi) + u_\varphi^m(s,z)\hat{\mathbf{e}}_\varphi(\varphi) + u_z^m(s,z)\hat{\mathbf{e}}_z\right]}_{=:\mathbf{u}_m(s,\varphi,z)} \mathrm{e}^{\mathrm{i}m\varphi}. \tag{1}$$

Equivalent expressions with $\sin\varphi$ and $\cos\varphi$ as used by Nissen-Meyer *et al.* (2007a) can be found by summing over pairs of $\pm m$ and using the fact that $\mathbf{u}$ is real. The question is whether the wave equation

$$\hat{\mathbf{K}}\mathbf{u} + \rho\partial_t^2\mathbf{u} = \mathbf{f} \tag{2}$$

in the expansion eq. (1) can be split into a series of independent equations, that is if there exist operators $\hat{\mathbf{K}}_m$ such that the set of equations

$$\hat{\mathbf{K}}_m\mathbf{u}_m + \rho\partial_t^2\mathbf{u}_m = \mathbf{f}_m \tag{3}$$

is equivalent to the wave equation eq. (2), where $\mathbf{f}_m$ denotes an expansion corresponding to eq. (1). While this is a well known fact for spherically symmetric earth models (which are a special case of axial symmetry and only include transversely isotropic media, see e.g. Dahlen & Tromp 1998), we prove here that this expansion is valid for a fully anisotropy medium, as long as it is azimuthally invariant:

$$c_{ijkl}(s,\varphi,z) = c_{ijkl}(s,z), \quad (i,j,k,l = s,\varphi,z). \tag{4}$$

In the normal mode context, this type of symmetry is often referred to as zonal symmetry (Dahlen & Tromp 1998).

2.2 Proof 1: Normal mode coupling due to zonally symmetric anisotropy

Nissen-Meyer *et al.* (2007a) show that the decomposition eq. (3) is valid for SNREI earth models and derive the series of equations explicitly for moment tensor and single force point sources on the polar axis, where m takes values between -2 and 2. Their argument was based on identification of the angular dependence in eq. (1) with analytic solutions of the wave equation using a normal mode expansion.

The strategy in this proof is to show that the angular dependence of the wavefield is not altered by the zonally symmetric anisotropy and hence the argument by Nissen-Meyer *et al.* (2007a) remains valid. After introducing the normal-mode solution, what remains to be shown is that only singlets with the same azimuthal dependence are coupled, as this leaves the total dependence on azimuth unchanged. This is equivalent to the selection rule $m = m'$, where m is the azimuthal order.

2.2.1 *A solution to the wave equation*

Consider the elastic wave equation eq. (2) where

$$\hat{\mathbf{K}}\mathbf{u} = -\boldsymbol{\nabla} \cdot (\mathbf{c} : \boldsymbol{\nabla}\mathbf{u}). \tag{5}$$

As $\hat{\mathbf{K}}$ is self-adjoint, it is diagonalizable in the space of square integrable functions L_2 on the domain Ω and the basis of eigenfunctions is orthogonalizable and countable (for more details refer to Woodhouse & Deuss 2007). Now assume any countable basis $\mathbf{s}^{(k)}$ of the L_2 that is orthonormal in the sense

$$\int_\Omega \rho \mathbf{s}^{(k)*} \cdot \mathbf{s}^{(k')}\, \mathrm{d}^3\mathbf{x} = \delta_{kk'}. \tag{6}$$

In this basis, eq. (2) can be written as an infinite dimensional matrix equation (Woodhouse 1983)

$$\mathbf{K}\mathbf{u} + \partial_t^2 \mathbf{u} = \mathbf{F}, \tag{7}$$

with the coupling matrix $\mathbf{K}$ having elements

$$\mathbf{K}_{kk'} = \int_\Omega \mathbf{s}^{(k)*} \cdot \hat{\mathbf{K}}\mathbf{s}^{(k')}\, \mathrm{d}^3\mathbf{x} \tag{8}$$

and the source vector $\mathbf{F}$ and $\mathbf{u}$ being the vector of coefficients for the displacement $\mathbf{u}$ in this basis. For an instantaneous point source, the coefficients of the source vector $\mathbf{F}$ are

$$\mathbf{F}_k = \left(\sum_i F_i s_i^{(k)}(\mathbf{r}_s) + \sum_{ij} M_{ij} \partial_j s_i^{(k)}(\mathbf{r}_s) \right) h(t), \tag{9}$$

where F_i are the components of a force vector, M_{ij} a moment tensor and $h(t)$ the Heaviside function. To avoid confusion, summation over repeated indices is always written explicitly throughout the paper. The solution to eq. (7) can then be written as (Woodhouse 1983)

$$\mathbf{u}(t) = \mathbf{K}^{-1} \left[1 - \cos\left(\sqrt{\mathbf{K}}t \right) \right] \mathbf{F}. \tag{10}$$

This time evolution is trivial, if $\mathbf{s}^{(km)}$ are eigenvectors of $\hat{\mathbf{K}}$, that is

$$\hat{\mathbf{K}}\mathbf{s}^{(km)} = \rho\omega_k^2 \mathbf{s}^{(km)}, \tag{11}$$

because then the coupling matrix $\mathbf{K}$ is diagonal. The additional index m accounts for possible degeneracy of the eigenfrequencies ω_k. In the case where $\hat{\mathbf{K}}$ is the elastic operator corresponding to the SNREI Earth, the set of eigenfunctions $\mathbf{s}^{(km)}$ corresponding to a degenerate eigenfrequency ω_k is called normal mode or the multiplet k. k then incorporates the angular order l, the overtone number n and the mode type (spheroidal or toroidal) and m is called the azimuthal order.

The problem of finding solutions to the wave equations is then reduced to finding eigenfrequencies and eigenvectors of the operator $\hat{\mathbf{K}}$, followed by application to a specific source and summation of the eigenfunctions according to eq. (10).

2.2.2 *Mode coupling selection rule $m = m'$*

While in the SNREI Earth the spherical parts of the eigenfunctions are found to be spherical harmonics, it is impractical to compute them explicitly in an Earth with lateral perturbations. A numerically exact solution can still be found by expressing $\hat{\mathbf{K}}$ in the normal mode basis and diagonalizing $\mathbf{K}$ numerically (Deuss & Woodhouse 2001). Once this is done, the eigenfunctions can be expressed in a normal mode sum as well. The time evolution is then nontrivial, because it is affected by coupling between modes.

To evaluate the elements of the coupling matrix, it is useful to express the strain $\mathbf{E}$ and the perturbed elastic stiffness tensor $c_{ijkl}(r, \theta, \varphi)$ in terms of generalized spherical harmonics Y_{lm}^N (Phinney & Burridge 1973; Dahlen & Tromp 1998, (C.164)):

$$\begin{aligned} \mathbf{E}^{(km)}(\mathbf{r}) &= \frac{1}{2}\left[\boldsymbol{\nabla}\mathbf{s}^{(km)}(\mathbf{r}) + \left(\boldsymbol{\nabla}\mathbf{s}^{(km)}(\mathbf{r})\right)^T \right] \\ &= \sum_{\alpha\beta} E_{km}^{\alpha\beta}(r) Y_{lm}^N(\theta,\varphi)\, \hat{\mathbf{e}}_\alpha \hat{\mathbf{e}}_\beta \end{aligned} \tag{12}$$

with $\alpha, \beta = -1, 0, 1$ and $N = \alpha + \beta$ and l is determined by k (see above). $\hat{\mathbf{e}}_{\alpha,\beta}$ are the canonical basis functions (Dahlen & Tromp 1998, (C.50))

$$\hat{\mathbf{e}}_{-1} = \frac{1}{\sqrt{2}}(\hat{\boldsymbol{\theta}} - \mathrm{i}\hat{\boldsymbol{\varphi}}), \quad \hat{\mathbf{e}}_0 = \hat{\mathbf{r}}, \quad \hat{\mathbf{e}}_{+1} = -\frac{1}{\sqrt{2}}(\hat{\boldsymbol{\theta}} + \mathrm{i}\hat{\boldsymbol{\varphi}}). \tag{13}$$

Similarly, we can write for the elastic tensor (Dahlen & Tromp 1998, (D.100)):

$$\boldsymbol{c}(\mathbf{r}) = \sum_{lm} \sum_{\alpha\beta\gamma\delta} c_{lm}^{\alpha\beta\gamma\delta}(r) Y_{lm}^N(\theta,\varphi)\, \hat{\mathbf{e}}_\alpha \hat{\mathbf{e}}_\beta \hat{\mathbf{e}}_\gamma \hat{\mathbf{e}}_\delta \tag{14}$$

with $\alpha, \beta, \gamma, \delta = -1, 0, 1$ and $N = \alpha + \beta + \gamma + \delta$. Zonal symmetry is then defined by $c_{lm}^{\alpha\beta\gamma\delta}(r) = 0$ if $m \neq 0$, that is the elastic tensor is independent of azimuth φ. The coupling matrix elements can then be written as (Woodhouse & Dahlen 1978; Dahlen & Tromp 1998, (D.115)):

$$\begin{aligned} &\langle km|\hat{\mathbf{K}}|k'm'\rangle \\ &= \int_\Omega \mathbf{s}^{(km)*} \cdot \hat{\mathbf{K}}\mathbf{s}^{(k'm')}\, \mathrm{d}^3\mathbf{x} \\ &= \int_\Omega \mathbf{E}^{(km)*} : \boldsymbol{c} : \mathbf{E}^{(k'm')}\, \mathrm{d}^3\mathbf{x} \\ &= \sum_{\alpha\beta\gamma\delta} \sum_{\gamma'\delta'} \sum_{st} \int_0^{r_0} E_{km}^{\alpha\beta *} c_{st}^{\alpha\beta\gamma\delta} E_{k'm'}^{\gamma'\delta'} g_{\gamma\gamma'} g_{\delta\delta'} r^2\, \mathrm{d}r \\ &\quad \times \int Y_{lm}^{N*} Y_{st}^{N+N'} Y_{l'm'}^{N'}\, \mathrm{d}\Omega, \end{aligned} \tag{15}$$

where $N = \alpha + \beta$, $N' = \gamma' + \delta'$ and g the metric tensor with $g_{00} = 1$, $g_{-11} = g_{1-1} = -1$ and $g_{\alpha\beta} = 0$ if $\alpha + \beta \neq 0$ and $\mathrm{d}\Omega$ the solid angle. Using the zonal symmetry ($t = 0$) and the definition of the generalized spherical harmonics (Phinney & Burridge 1973,

eq. (1.5)) the angular integral in eq. (15) can be expressed as

$$\begin{aligned}&\int Y_{lm}^{N*} Y_{s0}^{N+N'} Y_{l'm'}^{N'} \,\mathrm{d}\Omega \\ &= \int_0^{\pi} P_l^{Nm*}(\cos\theta) P_s^{(N+N')0}(\cos\theta) P_{l'}^{N'm'}(\cos\theta) \sin\theta \,\mathrm{d}\theta \\ &\quad \times \underbrace{\int_0^{2\pi} \mathrm{e}^{\mathrm{i}(m'-m)\varphi} \,\mathrm{d}\varphi}_{=0,\ \text{if } (m\neq m')} \\ &= 0 \qquad (m \neq m'). \end{aligned} \tag{16}$$

As no assumption about the elastic tensor c_{ijkl} was made apart from zonal symmetry, the selection rule $m = m'$ is a direct consequence of this symmetry independent of anisotropy. The advantage of this first proof is its rather intuitive perspective of mode coupling, but it has the disadvantage of relying on the decomposition into spherical harmonics and is hence limited to spherical domains.

2.3 Proof 2: Commuting operators

The second proof is more abstract but also more general as it is valid for all linear equations defined in the space of square integrable functions L_2 on domains Ω, if both the domain and the equation are invariant under rotations around a symmetry axis. For the seismic wave equation, this includes local domains as needed, for example for seismic exploration (suggested for explosive sources and isotropic media by Takenaka *et al.* 2003) and especially, as self-adjointness is not required, it readily includes linear viscoelasticity as well. Furthermore, this approach is applicable to a variety of other equations, for example the anisotropic acoustic wave equation that is frequently used in exploration geophysics (Alkhalifah 2000) or the Poisson and incompressible Stokes equations, see Bernardi *et al.* (1999) for a rigorous mathematical treatment. The method by Fournier *et al.* (2004) for the nonlinear Navier–Stokes equation is different in that it only treats axisymmetric solutions, while the solutions discussed here can take arbitrary form and the equation needs to have the symmetry.

Let $\Omega \subset \mathbb{R}^3$ and $\hat{\mathrm{T}}_\psi$ a rotation of the coordinate system by the angle ψ and Ω is invariant under the rotation. The action of $\hat{\mathrm{T}}_\psi$ on a function $\mathbf{u} : \Omega \to \mathbb{R}^3$ then is

$$\hat{\mathrm{T}}_\psi \mathbf{u}(\mathbf{x}) = \mathbf{R}_\psi \mathbf{u}\big(\mathbf{R}_\psi^T \mathbf{x}\big), \tag{17}$$

where $\mathbf{R}_\psi$ is the rotation matrix corresponding to the rotation around the symmetry axis of Ω. As stated above, any function $\mathbf{u} : \Omega \to \mathbb{R}^3$ that is square integrable can be expanded as in eq. (1). The basis vectors of the cylindrical coordinate system are symmetric with respect to the axis, that is $\hat{\mathrm{T}}_\psi \hat{\mathbf{e}}_{\{s,\varphi,z\}} = \hat{\mathbf{e}}_{\{s,\varphi,z\}}$. The action of the rotation operator in this decomposition therefore simplifies to

$$\hat{\mathrm{T}}_\psi \left(\mathbf{u}_m(s,\varphi,z)\mathrm{e}^{\mathrm{i}m\varphi}\right) = \mathrm{e}^{-\mathrm{i}m\psi}\mathbf{u}_m(s,\varphi,z)\mathrm{e}^{\mathrm{i}m\varphi}. \tag{18}$$

Now consider the equation

$$\hat{\mathrm{H}}\mathbf{u} = \mathbf{f}, \tag{19}$$

where the operator $\hat{\mathrm{H}}$ is linear, the equation has a unique non-trivial solution $\mathbf{u}$ and $\hat{\mathrm{H}}$ commutes with $\hat{\mathrm{T}}_\psi$, that is

$$\hat{\mathrm{H}}\hat{\mathrm{T}}_\psi \mathbf{u} = \hat{\mathrm{T}}_\psi \hat{\mathrm{H}}\mathbf{u}, \qquad \text{for all } \mathbf{u} \in L_2. \tag{20}$$

In other words, whether the function is first rotated and $\hat{\mathrm{H}}$ is applied subsequently or $\hat{\mathrm{H}}$ is applied first and the resulting function then rotated does not affect the final result. In the case of the elastic wave equation, $\hat{\mathrm{H}}$ is the elastodynamic operator $\hat{\mathrm{K}} + \rho\partial_t^2$ which fulfills these criteria if the medium is symmetric with respect to the z-axis, see eq. (4).

Similar to $\mathbf{u}$, the source $\mathbf{f}$ has a decomposition as in eq. (1) with $\mathbf{f} = \sum_{m'} \mathbf{f}_{m'} \mathrm{e}^{\mathrm{i}m'\varphi}$ and the behaviour under rotation as in eq. (18). Because of the linearity of $\hat{\mathrm{H}}$, we can first consider solutions for $\hat{\mathrm{H}}\mathbf{u} = \mathbf{f}_{m'}\mathrm{e}^{\mathrm{i}m'\varphi}$ and sum over m' later. If we apply the rotation $\hat{\mathrm{T}}_\psi$ to the linear wave equation and use the commuting property, we have

$$\hat{\mathrm{H}}\hat{\mathrm{T}}_\psi \mathbf{u} = \mathrm{e}^{-\mathrm{i}m'\psi}\mathbf{f}_{m'}\mathrm{e}^{\mathrm{i}m'\varphi}. \tag{21}$$

Using the uniqueness of the solution and linearity of $\hat{\mathrm{H}}$ this implies

$$\hat{\mathrm{T}}_\psi \mathbf{u} = \mathrm{e}^{-\mathrm{i}m'\psi}\mathbf{u} = \mathrm{e}^{-\mathrm{i}m'\psi} \sum_{m=-\infty}^{\infty} \mathbf{u}_m \mathrm{e}^{\mathrm{i}m\varphi}. \tag{22}$$

On the other hand, using eq. (18):

$$\hat{\mathrm{T}}_\psi \mathbf{u} = \sum_{m=-\infty}^{\infty} \mathrm{e}^{-\mathrm{i}m\psi}\mathbf{u}_m \mathrm{e}^{\mathrm{i}m\varphi}. \tag{23}$$

Because of the orthogonality of $\mathrm{e}^{-\mathrm{i}m\psi}$, both relations can hold at the same time and for all ψ if and only if

$$\mathbf{u}_m = 0, \quad (\text{for all } m \neq m'). \tag{24}$$

In conclusion, eq. (19) can be separated into a series of independent equations

$$\hat{\mathrm{H}}\mathbf{u}_m \mathrm{e}^{\mathrm{i}m\varphi} = \mathbf{f}_m \mathrm{e}^{\mathrm{i}m\varphi}, \qquad (m \in \mathbb{N}). \tag{25}$$

An equivalent set of reduced equations with functions $\tilde{\mathbf{u}}_m(s,z)$ and $\tilde{\mathbf{f}}_m(s,z)$ defined on Ω_D with $\Omega = \Omega_D \otimes [0, 2\pi]$ can be defined such that

$$\hat{\mathrm{H}}_m \tilde{\mathbf{u}}_m(s,z) = \tilde{\mathbf{f}}_m(s,z), \qquad (m \in \mathbb{N}). \tag{26}$$

These are derived explicitly for $m = 0, \pm 1, \pm 2$ (as these are the only contributions for a moment tensor or single force point source on the symmetry axis) for the wave equation in the isotropic elastic and fluid cases in sections 4.5–4.6 and appendix in Nissen-Meyer *et al.* (2007a) and will be presented in the next section for the anisotropic elastic case.

3 THE AXISYMMETRIC SYSTEM

3.1 Equations of motion

In this section, we derive the equations of motions of the reduced 2-D equations in the weak form explicitly. This step essentially consists of projecting the wave equation onto test functions having the azimuthal dependence of monopole, dipole and quadrupole sources as defined in eq. (1). Taking the dot product of eq. (2) with a test function $\mathbf{w}$, integrating over the domain Ω and using partial integration and the free surface boundary condition yields

$$\int_\Omega \Big(\underbrace{\rho\mathbf{w}\cdot\ddot{\mathbf{u}}}_{\text{mass}} + \underbrace{\nabla\mathbf{w} : (\boldsymbol{c} : \nabla\mathbf{u})}_{\text{stiffness}} \Big) \,\mathrm{d}^3\mathbf{x} = \int_\Omega \underbrace{\mathbf{w}\cdot\mathbf{f}}_{\text{force}} \,\mathrm{d}^3\mathbf{x}. \tag{27}$$

If this equation holds for all $\mathbf{w}$, this so called weak form is equivalent to the original wave equation. When inserting the specific dependence of the wavefield $\mathbf{u}$ and the test function $\mathbf{w}$ on the azimuth φ, the integral in φ can be solved analytically leaving only the integral over the 2-D semicircular domain Ω_D, see Fig. 1. The domain Ω of interest here is the solid part of the Earth, for the full solid-fluid system see Nissen-Meyer *et al.* (2008). Both source and mass term are independent of the elastic tensor $\boldsymbol{c}$, so we only consider the stiffness terms to generalize eqs (5)–(7) in Nissen-Meyer *et al.* (2007b) to anisotropic earth models.

3.1.1 Stiffness terms

For the monopole ($m = 0$), integrating the stiffness terms over φ results in (omitting the integral over Ω_D on both sides)

$$\begin{aligned}
&\frac{1}{2\pi}\int_0^{2\pi} \nabla\mathbf{w} : (\boldsymbol{c} : \nabla\mathbf{u})\, \mathrm{d}\varphi \\
&= \partial_s w_s \left(C_{11}\partial_s u_s + C_{13}\partial_z u_z + C_{15}(\partial_s u_z + \partial_z u_s) + C_{12}\frac{u_s}{s}\right) \\
&\quad + \partial_z w_s \left(C_{15}\partial_s u_s + C_{35}\partial_z u_z + C_{55}(\partial_s u_z + \partial_z u_s) + C_{25}\frac{u_s}{s}\right) \\
&\quad + \frac{1}{s} w_s \left(C_{12}\partial_s u_s + C_{23}\partial_z u_z + C_{25}(\partial_s u_z + \partial_z u_s) + C_{22}\frac{u_s}{s}\right) \\
&\quad + \partial_s w_z \left(C_{15}\partial_s u_s + C_{35}\partial_z u_z + C_{55}(\partial_s u_z + \partial_z u_s) + C_{25}\frac{u_s}{s}\right) \\
&\quad + \partial_z w_z \left(C_{13}\partial_s u_s + C_{33}\partial_z u_z + C_{35}(\partial_s u_z + \partial_z u_s) + C_{23}\frac{u_s}{s}\right),
\end{aligned} \tag{28}$$

where C_{ij} is the elastic tensor c_{ijkl} in Voigt notation with the index mapping

$$\begin{aligned}
&\{ss\} \to 1, \qquad \{\varphi\varphi\} \to 2, \qquad \{zz\} \to 3, \\
&\{\varphi z\} \to 4, \qquad \{zs\} \to 5, \qquad \{s\varphi\} \to 6.
\end{aligned} \tag{29}$$

Equivalent expressions for dipole and quadrupole sources can be found in the Appendix A. At this point we have carried out the integration in azimuth in eq. (27) and end up with an equation of motion in the weak form with a domain of definition that spans the semi-circular domain Ω_D, see Fig. 1.

3.1.2 Effective elasticity tensor

Inspection of eqs (28, A2, A3) reveals that 8 out of the 21 independent coefficients in the elasticity tensor drop out in the integration of the stiffness terms over φ for all source types, namely C_{14}, C_{24}, C_{34}, C_{16}, C_{26}, C_{36}, C_{45}, C_{56}. These are exactly the coefficients that are antisymmetric with respect to the s-z plane, that is change sign under coordinate transform $\varphi \to -\varphi$. By setting these coefficients to zero, an effective elasticity tensor can be defined that is symmetric with respect to the s–z plane, that is invariant under coordinate transform $\varphi \to -\varphi$.

In practice, this means that recorded seismic waveforms of a specific source–receiver combination are fundamentally insensitive to these antisymmetric coefficients so long as the 2.5-D approximation is valid, that is for structural variations on a larger scale than the Fresnel zone. To image full anisotropy using high-frequency body waves, multiple crossings of a certain region are therefore necessary not only for spatial resolution as in isotropic imaging, but also to resolve the full elastic tensor.

3.2 Discretization

The next step is to generalize the spatial discretization of the stiffness terms from the isotropic case presented in Nissen-Meyer *et al.* (2007b) to the anisotropic case. The approach is the same as in the isotropic case and we refer the reader to section 3 in Nissen-Meyer *et al.* (2007b) for details and restrict ourselves to a short summary of the method and important aspects of the notation in the interest of brevity.

The collapsed 2-D domain Ω_D is divided into non-axial elements Ω_e and axial elements $\Omega_{\bar{e}}$. The mapping between reference coordinates $\xi, \eta \in [-1, 1]$ in each element and the physical coordinates s, z is provided by the Jacobian determinant

$$\mathcal{J}(\xi, \eta) = \det\begin{pmatrix} s_\xi & s_\eta \\ z_\xi & z_\eta \end{pmatrix}, \tag{30}$$

where the subscript denotes partial derivation, $s_\xi = \partial_\xi s$ etc. Both the test function $\mathbf{w}$ and the displacement $\mathbf{u}$ are expanded in Lagrangian polynomials l_i of order N (defined on the integration points, see below) within each element

$$u^\alpha(\xi, \eta, t) = \sum_{ij} u^\alpha_{ij}(t) l_i(\xi) l_j(\eta) \tag{31}$$

for each component $\alpha \in (s, \varphi, z)$ and equivalently for $\mathbf{w}$. For the axial elements $\xi = 0$ is the axis. The integral over the domain Ω_D is then split into a sum of integrals over elements and approximated using the Gauss Lobatto integration rule

$$\int_{\Omega_e} u(s, z) s \, \mathrm{d}s \, \mathrm{d}z \approx \sum_{pq} \sigma_p \sigma_q s(\xi_p, \eta_q) u_{pq} \mathcal{J}(\xi_p, \eta_q) \tag{32}$$

with Gauss Lobatto Legendre (GLL) integration weights σ_p and integration points ξ_p and η_q. For the axial elements, Gauss Lobatto Jacobi (GLJ) quadrature is used for the ξ direction with

$$\int_{\Omega_{\bar{e}}} u(s, z) s \, \mathrm{d}s \, \mathrm{d}z \approx \sum_{pq} \bar{\sigma}_p (1 + \bar{\xi}_p)^{-1} \sigma_q s(\bar{\xi}_p, \eta_q) u_{pq} \mathcal{J}(\bar{\xi}_p, \eta_q) \tag{33}$$

and GLJ integration weights $\bar{\sigma}_p$, integration points $\bar{\xi}_p$ and the Lagrangian interpolation polynomial on these points $\bar{l}(\xi)$. This allows to use l'Hospital's rule to calculate derivatives at the axis where needed.

Applying this discretization to eq. (27), choosing the set of test functions to be 1 in one component at a specific integration point and 0 at the others and summing over all elements we obtain the global set of ordinary differential equations in time

$$\mathbf{M}\ddot{\mathbf{u}}(t) + \mathbf{K}\mathbf{u}(t) = \mathbf{f}(t), \tag{34}$$

with the global mass matrix $\mathbf{M}$ and stiffness matrix $\mathbf{K}$. While the assembled mass matrix is diagonal in the GLL/GLJ basis (hence trivial to invert), it is unnecessary to compute $\mathbf{K}$ explicitly and we only evaluate its action on the displacement ($\mathbf{Ku}$). This term only appears on the right hand side of the second order system

$$\ddot{\mathbf{u}}(t) = \mathbf{M}^{-1}[\mathbf{f}(t) - \mathbf{K}\mathbf{u}(t)] \tag{35}$$

which is solved by explicit numerical time integration schemes. The stiffness terms $\mathbf{Ku}$ are solved in each element first and the global stiffness is assembled subsequently (Nissen-Meyer *et al.* 2007b, section 4).

The only difference compared to the isotropic case is in the elemental stiffness terms, which we derive here for the anisotropic case. We split the original elemental stiffness integral into contributions from each component β of the vectorial test function $\mathbf{w}$, denoted by the subscript β. Furthermore, we split the contributions from terms in eq. (28) with two ('leading order') or less ('lower order') partial derivatives, denoted by superscripts $\partial\partial$ and ∂. The full elemental stiffness for the monopole is hence split as

$$\mathbf{Ku} = \sum_{\beta \in \{s,z\}} \left((\mathbf{Ku})^{\partial\partial}_\beta + (\mathbf{Ku})^{\partial}_\beta\right). \tag{36}$$

Furthermore, we revert to a tensorial notation instead of elemental sums and define the matrix–matrix products

$$\begin{aligned}
\mathbf{X} = \mathbf{A} \otimes \mathbf{B}: &\qquad X_{ij} = \sum_k A_{ik} B_{kj} \\
\mathbf{X} = \mathbf{A} \odot \mathbf{B}: &\qquad X_{ij} = A_{ij} B_{ij}
\end{aligned} \tag{37}$$

and vector–matrix and vector–vector products

$$\begin{aligned}
\mathbf{X}^0 = \mathbf{A}^0 \otimes \mathbf{B}: &\qquad X_{0j} = \sum_k A_{0k} B_{kj} \\
\mathbf{X}^0 = \mathbf{A}^0 \odot \mathbf{B}^0: &\qquad X_{0j} = A_{0j} B_{0j} \\
\mathbf{X} = \mathbf{A}^0 \mathbf{B}^0: &\qquad X_{ij} = A_{i0} B_{0j}.
\end{aligned} \tag{38}$$

The leading order terms have contributions from the components α of the displacement $\mathbf{u}$, where the φ component vanishes for the monopole source, thus

$$(\mathbf{Ku})^{\partial\partial}_{\beta} = \sum_{\alpha \in \{s,z\}} (\mathbf{Ku})^{\partial\partial}_{\beta\alpha}, \tag{39}$$

with

$$\begin{aligned}
(\mathbf{Ku})^{\partial\partial}_{\beta\alpha} = {} & \mathbf{D}_\xi \otimes \left[\mathbf{C} \odot \mathbf{E}^{(1)}_{\beta\alpha} \odot \left(\mathbf{u}_\alpha \otimes \mathbf{D}_\eta\right)\right] \\
& + \mathbf{D}_\xi \otimes \left[\mathbf{C} \odot \mathbf{E}^{(2)}_{\beta\alpha} \odot \left(\mathbf{D}_\xi^{\mathrm{T}} \otimes \mathbf{u}_\alpha\right)\right] \\
& + \left[\mathbf{C} \odot \mathbf{E}^{(3)}_{\beta\alpha} \odot \left(\mathbf{D}_\xi^{\mathrm{T}} \otimes \mathbf{u}_\alpha\right)\right] \otimes \mathbf{D}_\eta^{\mathrm{T}} \\
& + \left[\mathbf{C} \odot \mathbf{E}^{(4)}_{\beta\alpha} \odot \left(\mathbf{u}_\alpha \otimes \mathbf{D}_\eta\right)\right] \otimes \mathbf{D}_\eta^{\mathrm{T}}.
\end{aligned} \tag{40}$$

with $\mathbf{C}$ and $\mathbf{D}$ from Table 1 and $\mathbf{E}^{(k)}_{\beta\alpha}$ defined as:

$$\begin{aligned}
\mathbf{E}^{(k)}_{ss} &= {}_{C_{11}}\mathbf{G}^{ss}_k + {}_{C_{15}}\mathbf{G}^{sz}_k + {}_{C_{15}}\mathbf{G}^{zs}_k + {}_{C_{55}}\mathbf{G}^{zz}_k \\
\mathbf{E}^{(k)}_{sz} &= {}_{C_{15}}\mathbf{G}^{ss}_k + {}_{C_{13}}\mathbf{G}^{sz}_k + {}_{C_{55}}\mathbf{G}^{zs}_k + {}_{C_{35}}\mathbf{G}^{zz}_k \\
\mathbf{E}^{(k)}_{zs} &= {}_{C_{15}}\mathbf{G}^{ss}_k + {}_{C_{55}}\mathbf{G}^{sz}_k + {}_{C_{13}}\mathbf{G}^{zs}_k + {}_{C_{35}}\mathbf{G}^{zz}_k \\
\mathbf{E}^{(k)}_{zz} &= {}_{C_{55}}\mathbf{G}^{ss}_k + {}_{C_{35}}\mathbf{G}^{sz}_k + {}_{C_{35}}\mathbf{G}^{zs}_k + {}_{C_{33}}\mathbf{G}^{zz}_k
\end{aligned} \tag{41}$$

with ${}_\epsilon\mathbf{G}^{xy}_k$ from Table 1. Defining

$$\begin{aligned}
\mathbf{M}_1 &= {}_{C_{12}}\mathbf{B}_{z_\eta} + {}_{C_{25}}\mathbf{B}_{s_\eta} \qquad & \mathbf{M}_2 &= {}_{C_{12}}\mathbf{B}_{z_\xi} + {}_{C_{25}}\mathbf{B}_{s_\xi} \\
\mathbf{M}_3 &= {}_{C_{25}}\mathbf{B}_{z_\eta} + {}_{C_{23}}\mathbf{B}_{s_\eta} \qquad & \mathbf{M}_4 &= {}_{C_{25}}\mathbf{B}_{z_\xi} + {}_{C_{23}}\mathbf{B}_{s_\xi} \\
\mathbf{M}_{w1} &= {}_{C_{22}}\mathbf{A} \\
\mathbf{M}^0_{w1} &= {}_{(2C_{12}+C_{22})}\mathbf{A}^0 \qquad & \mathbf{M}^0_{w2} &= {}_{C_{25}}\mathbf{A}^0 \\
\mathbf{M}^0_{w3} &= {}_{C_{25}}\mathbf{B}^0_{z_\xi} + {}_{C_{23}}\mathbf{B}^0_{s_\xi}
\end{aligned} \tag{42}$$

with ${}_\epsilon\mathbf{A}$ and ${}_\epsilon\mathbf{B}_{x_\zeta}$ from Table 1 the lower-order terms read:

$$\begin{aligned}
(\mathbf{Ku})^{\partial}_{s} = {} & \mathbf{D}_\xi \otimes (\mathbf{M}_1 \odot \mathbf{u}_s) + (\mathbf{M}_2 \odot \mathbf{u}_s) \otimes \mathbf{D}_\eta^{\mathrm{T}} \\
& + \mathbf{M}_1 \odot \left(\mathbf{D}_\xi^{\mathrm{T}} \otimes \mathbf{u}_s\right) + \mathbf{M}_3 \odot \left(\mathbf{D}_\xi^{\mathrm{T}} \otimes \mathbf{u}_z\right) \\
& + \mathbf{M}_2 \odot \left(\mathbf{u}_s \otimes \mathbf{D}_\eta\right) + \mathbf{M}_4 \odot \left(\mathbf{u}_z \otimes \mathbf{D}_\eta\right) \\
& + \mathbf{M}_{w1} \odot \mathbf{u}_s \\
& + \delta_{e\bar{e}} \mathbf{D}^0_\xi \Big[\mathbf{M}^0_{w3} \odot \left(\mathbf{u}^0_z \otimes \mathbf{D}_\eta\right) \\
& \qquad + \mathbf{M}^0_{w1} \odot \left(\left(\mathbf{D}^0_\xi\right)^{\mathrm{T}} \otimes \mathbf{u}_s\right) \\
& \qquad + \mathbf{M}^0_{w2} \odot \left(\left(\mathbf{D}^0_\xi\right)^{\mathrm{T}} \otimes \mathbf{u}_z\right)\Big]
\end{aligned} \tag{43}$$

$$\begin{aligned}
(\mathbf{Ku})^{\partial}_{z} = {} & \mathbf{D}_\xi \otimes (\mathbf{M}_3 \odot \mathbf{u}_s) + (\mathbf{M}_4 \odot \mathbf{u}_s) \otimes \mathbf{D}_\eta^{\mathrm{T}} \\
& + \delta_{e\bar{e}} \Big\{\mathbf{D}^0_\xi \Big[\mathbf{M}^0_{w2} \odot \left(\left(\mathbf{D}^0_\xi\right)^{\mathrm{T}} \otimes \mathbf{u}_s\right)\Big] \\
& \qquad + \Big[\mathbf{M}^0_{w3} \odot \left(\left(\mathbf{D}^0_\xi\right)^{\mathrm{T}} \otimes \mathbf{u}_s\right)\Big] \otimes \mathbf{D}_\eta^{\mathrm{T}}\Big\}.
\end{aligned} \tag{44}$$

Here $\delta_{e\bar{e}}$ is 1 in axial elements and 0 otherwise and is used to denote the additional terms that occur from the special treatment of derivatives at the axis.

Importantly, the computational cost is not increased measurably within the time-evolution compared to the isotropic version: in the monopole case the only additional term is the 1-D axial term with $\mathbf{M}^0_{w2}$. $\mathbf{E}_{\beta\alpha}$ receives additional contributions, but these are

Table 1. Definitions for pre-computable matrices (that is, prior to the costly time extrapolation) of the stiffness terms, $\pm$ takes its value depending on the combination of x_ζ as in the lower right table. Subscript reference coordinates denotes partial derivation, $x_\zeta = \partial_\zeta x$. For consistency with the summation notation in Nissen-Meyer *et al.* (2007a), we use indices i, j and I, J, which all take the values in $[0, N]$.

Matrix	Non-axial elements	Axial elements ($i > 0$)	($i = 0$)	Axial vectors
$({}_\epsilon\mathbf{A})^{ij}$	$\epsilon^{ij}\sigma_i\sigma_j(s^{ij})^{-1}\mathcal{J}^{ij}$	$\epsilon^{ij}\bar{\sigma}_i(1+\bar{\xi}_i)^{-1}\sigma_j(s^{ij})^{-1}\mathcal{J}^{ij}$	0	$({}_\epsilon\mathbf{A}^0)^j = \epsilon^{0j}\bar{\sigma}_0\sigma_j\mathcal{J}^{0j}\left(s^{0j}_\xi\right)^{-1}$
$({}_\epsilon\mathbf{B}_{x_\zeta})^{ij}$	$\pm\epsilon^{ij}\sigma_i\sigma_j x^{ij}_\zeta$	$\pm\epsilon^{ij}\bar{\sigma}_i(1+\bar{\xi}_i)^{-1}\sigma_j x^{ij}_\zeta$	0	$\left({}_\epsilon\mathbf{B}^0_{x_\zeta}\right)^j = \pm\epsilon^{0j}\bar{\sigma}_0\sigma_j x^{0j}_\zeta$
$(\mathbf{C})^{ij}$	$\sigma_i\sigma_j s^{ij}(\mathcal{J}^{ij})^{-1}$	$\bar{\sigma}_i\sigma_j s^{ij}(1+\bar{\xi}_i)^{-1}(\mathcal{J}^{ij})^{-1}$	0	$(\mathbf{C}^0)^j = \bar{\sigma}_0\sigma_j s^{0j}_\xi(\mathcal{J}^{0j})^{-1}$
$(\mathbf{D}_\xi)^{Ii}$	$\partial_\xi l_I(\xi_i)$	$\partial_\xi \bar{l}_I(\bar{\xi}_i)$	$\partial_\xi \bar{l}_I(\bar{\xi}_0)$	$\left(\mathbf{D}^0_\xi\right)^I = \partial_\xi \bar{l}_I(\bar{\xi}_0)$
$\left(\mathbf{D}_\eta\right)^{Jj}$	$\partial_\eta l_J(\eta_j) = \partial_\xi l_J(\xi_j)$	$\partial_\eta l_J(\eta_j)$		

$\left({}_\epsilon\mathbf{G}^{xy}_k\right)^{ij}$	$k=1$	$k=2$	$k=3$	$k=4$
$x=s, y=s$	$-z^{ij}_\xi z^{ij}_\eta \epsilon^{ij}$	$z^{ij}_\eta z^{ij}_\eta \epsilon^{ij}$	$-z^{ij}_\xi z^{ij}_\eta \epsilon^{ij}$	$z^{ij}_\xi z^{ij}_\xi \epsilon^{ij}$
$x=s, y=z$	$z^{ij}_\eta s^{ij}_\xi \epsilon^{ij}$	$-z^{ij}_\eta s^{ij}_\eta \epsilon^{ij}$	$z^{ij}_\xi s^{ij}_\eta \epsilon^{ij}$	$-z^{ij}_\xi s^{ij}_\xi \epsilon^{ij}$
$x=z, y=s$	$s^{ij}_\eta z^{ij}_\xi \epsilon^{ij}$	$-s^{ij}_\eta z^{ij}_\eta \epsilon^{ij}$	$s^{ij}_\xi z^{ij}_\eta \epsilon^{ij}$	$-s^{ij}_\xi z^{ij}_\xi \epsilon^{ij}$
$x=z, y=z$	$-s^{ij}_\xi s^{ij}_\eta \epsilon^{ij}$	$s^{ij}_\eta s^{ij}_\eta \epsilon^{ij}$	$-s^{ij}_\xi s^{ij}_\eta \epsilon^{ij}$	$s^{ij}_\xi s^{ij}_\xi \epsilon^{ij}$

$\pm(x_\zeta)$	$\zeta = \xi$	$\zeta = \eta$
$x = s$	$+$	$-$
$x = z$	$-$	$+$

pre-computed before the time loop (Table 1). This is similar for dipole and quadrupole sources (see Appendix), so we dropped the isotropic implementation and use the new anisotropic version as well for entirely isotropic models.

4 BENCHMARKS

Solving the full 3-D wave equation for arbitrary earthquake sources in axisymmetric models, *AxiSEM* seems to be unique among the available codes. For benchmarking we thus have to revert to spherically symmetric models, but as the code is written in cylindrical coordinates, even transversely isotropic media lead to a stiffness tensor that is fully populated (those elements that are nonzero in the effective stiffness tensor, see above) and the full stiffness matrix is tested. As a reference, we use *Yspec* by Al-Attar & Woodhouse (2008), which is a generalization of the direct radial integration method (Friederich & Dalkolmo 1995) including self-gravitation (switched off for the benchmark).

4.1 High frequency seismograms

While Nissen-Meyer *et al.* (2008) could only perform benchmarks down to 20 s period due to limitations in the reference normal mode solution, this limit is overcome using *Yspec*. Also, *AxiSEM* since then has experienced some substantial development (Nissen-Meyer *et al.* 2014), specifically the improved parallelization allows us to perform production runs up to the highest frequencies observed for global body waves.

Fig. 2 shows a record section of seismograms computed for the anisotropic PREM model (Dziewonski & Anderson 1981) with continental crust computed with *Yspec* and *AxiSEM*. The source is a strike slip event with a moment magnitude $M_w = 5.0$ in 117 km depth under Oaxaca, Mexico. The traces recorded at some selected GSN stations are filtered between 5 and 1 s. Due to the high-frequency content, it is necessary to zoom in to see any differences at all: the agreement between the two methods is remarkable even though the highest frequencies have traveled more than 1000 wavelengths (given the low pass filter at 1 s, the time axis is equivalent to the number of travelled wavelengths).

We use the phase and envelope misfit (*PM* and *EM* as defined by Kristekova *et al.* 2009) for quantitative comparison within the zoom windows and find phase misfits well below 1 per cent for all windows and envelope misfits below 1.1 per cent for all windows but the extremely small amplitude phase ScS at JTS, where it reaches a maximum of 2.3 per cent. Errors in amplitude and phase are therefore negligibly small compared to other errors when comparing these synthetics to data like, for example noise or the assumption of a 1-D model.

The total cost of this run with *AxiSEM* was about 70 K CPU hours using a fourth order symplectic time scheme (Nissen-Meyer *et al.* 2008) on a Cray XE6. The mesh was built for periods down to 0.8 s and the time step chosen 30 per cent below the CFL criterion, as this run was meant to prove convergence to the same result as *Yspec*. In applications where less accuracy is necessary one could either use the same traces at higher frequencies or reduce this cost substantially by choosing a larger time step and a coarser mesh.

4.2 Low frequency spectra

Normal mode eigenfrequency and phase spectra are extremely sensitive to Earth's structure, so they also provide a good benchmark at the low frequency end of the spectrum. For the comparison, 48 hr of synthetic seismogram were tapered with a cosine function and transformed to the frequency domain. Fig. 3 shows both amplitude and phase spectra with a zoom on the frequencies just above 5 mHz. The agreement in the amplitude spectrum is striking and there is essentially no visible difference. The phase spectra agree slightly less well compared to the amplitudes due to accumulated dispersion errors in the time stepping of *AxiSEM* (1.7 million time steps with a 2nd order Newmark time scheme, equivalent to 2000 propagated wavelengths at $\approx$10 mHz), but the most visible differences (e.g. around 5.4 mHz) arise from phase wrapping at π, $-\pi$.

In summary, our validation against an entirely different approach (frequency versus time domain, 1-D versus 2.5-D modelling) at the high- and low end of the relevant frequency spectrum of global seismology is outstanding. To the best of our knowledge no such benchmarks between two entirely different codes for both 1 Hz wave propagation or for mode spectra have been published.

5 APPLICATIONS

Hemispherical structure in the inner core of the Earth is well documented (e.g. Morelli *et al.* 1986; Creager 1992; Irving *et al.* 2008, 2009; Deuss *et al.* 2010; Waszek & Deuss 2011), where the Eastern Hemisphere is nearly isotropic and faster on average and the Western Hemisphere is anisotropic and slower than average. The observed anisotropy is of hexagonal symmetry with a fast axis approximately parallel to the rotation axis of the Earth and a slow plane parallel to the equator. Anisotropy is an important diagnostic property of the inner core since it allows to impose constraints on super-rotation (Waszek *et al.* 2011) and the history of inner core formation.

Inner core body waves are typically observed at frequencies around 0.5–2.0 Hz, which is unfeasible for 3-D-discretized global seismic wave simulations. On the other hand, due to the high frequencies, the Fresnel zones are very narrow and for the early arriving inner core phases off-path scattering can be neglected. The 2.5-D approximation is hence likely valid, if the medium parameters vary slowly perpendicular to the source receiver plane. Using high-frequency synthetics computed with *AxiSEM* one can study the problem in terms of waveform effects, potentially allowing for additional insights compared to solely analysing ray-theoretical traveltimes. Furthermore, there is an epicentral distance region around 146° where PKPab, PKPbc and PKiKP phases arrive at the receiver at the same time, see Fig. 4. This distance region corresponds to a depth region of turning rays, where traveltime cannot be extracted with classical ray-theoretical methods. Having full waveforms computed with *AxiSEM* at hand, extracting additional information about this depth region could help further constrain inner core structure.

Fig. 4 shows a record section zoomed in to the inner core phases for an explosive source beneath the North pole, bandpass filtered from 1 to 2 Hz. The background model is isotropic PREM for the black traces and includes hexagonal anisotropy in the inner core with the fast axis in north–south direction for the red traces. This represents a model according to results for uniform anisotropy by Irving & Deuss (2011). This model is represented exactly in the 2.5-D modeling of *AxiSEM*, the validity of the 2.5-D approximation for more general models will be subject to future parameter studies. As a reference, major ray-theoretical arrivals in PREM are indicated with blue lines, *PKIKP* and *pPKIKP* for the anisotropic core with green lines.

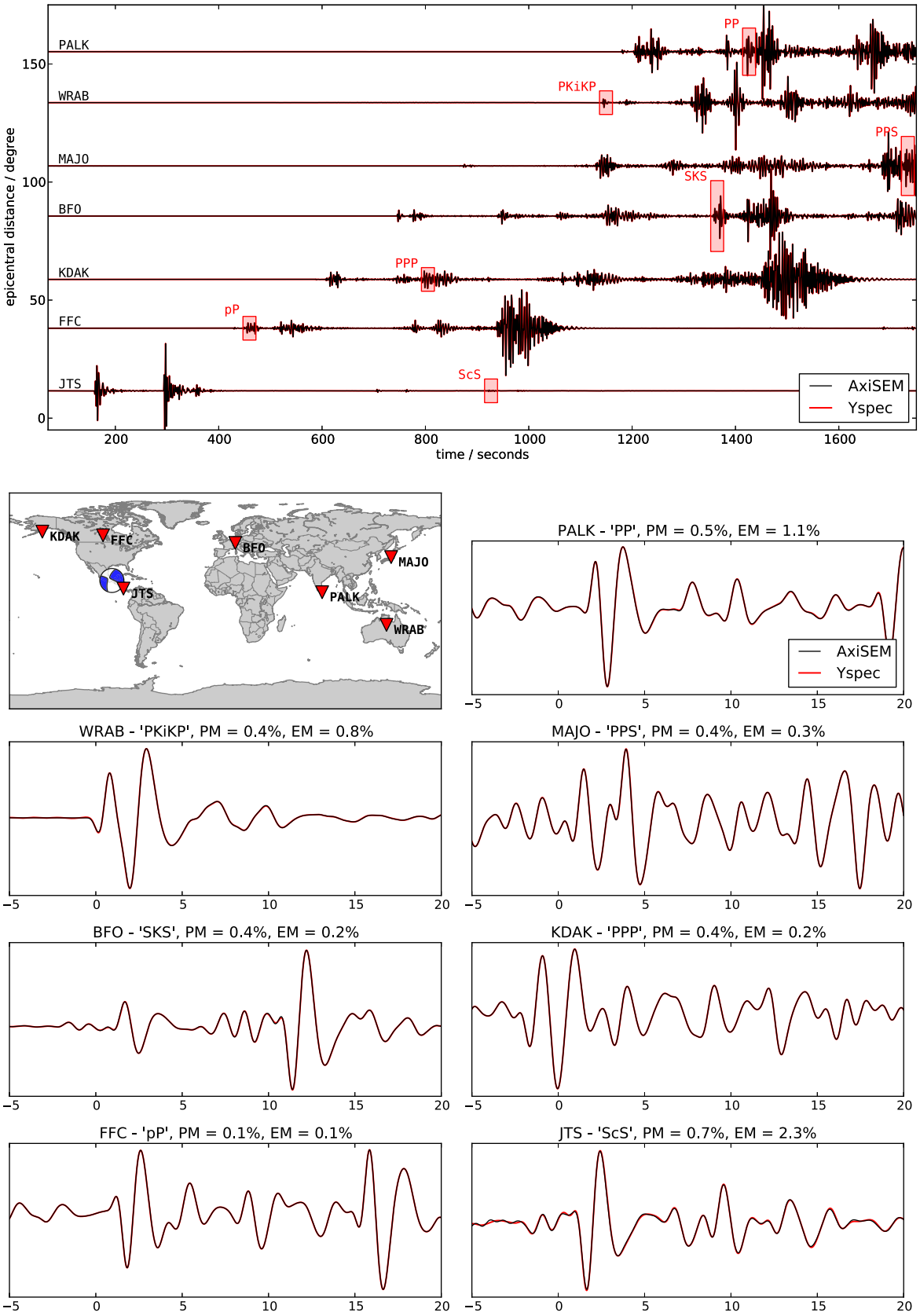

Figure 2. Comparison of vertical displacement seismograms (band pass filtered from 5 to 1 s period) for a strike slip event with a moment magnitude $M_w = 5.0$ in 117 km depth under Oaxaca, Mexico, computed with *AxiSEM* and *Yspec* in the anisotropic PREM model without ocean. The traces are recorded at the GSN stations indicated in the map. The zoom windows are indicated with red rectangles in the record section and the time scale is relative to the ray-theoretical arrival. *EM* and *PM* denote the envelope and phase misfit in the time window plotted (Kristekova *et al.* 2009).

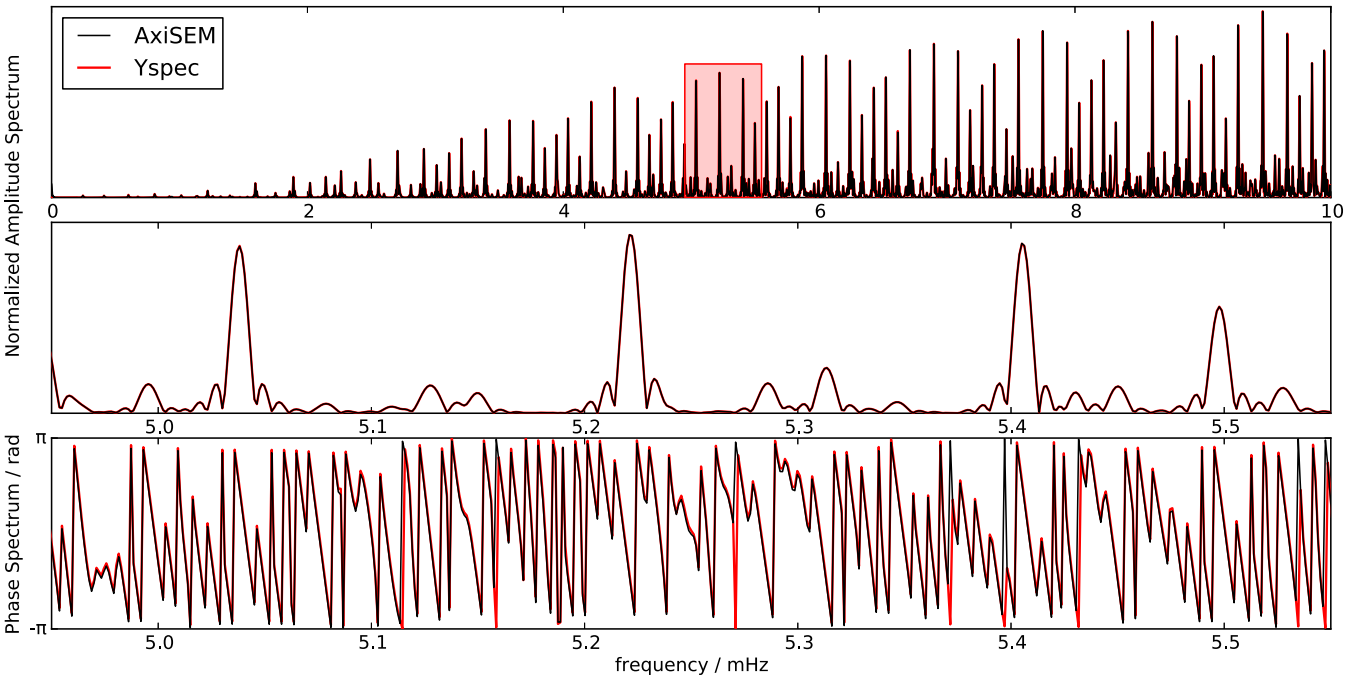

Figure 3. Comparison of amplitude- and phase-spectra of 48 hr time-series generated with *AxiSEM* and *Yspec*, lower two are zooms into the region marked with the red rectangle. Most differences that appear to be large in the phase spectrum (e.g. just below 5.3 mHz) are actually small and are visible only because of phase wrapping at π, $-\pi$.

Ray-theoretical traveltimes for *PKIKP* and *pPKIKP* in the anisotropic model can be computed using the small anisotropy approximation for the perturbation of the *P*-wave velocity as a function of the ray angle ζ between the fast axis and the direction of wave propagation (Morelli *et al.* 1986):

$$\frac{\delta v_p(\zeta)}{v_p} = a + b\cos^2\zeta + c\cos^4\zeta, \tag{45}$$

where v_p is the *P*-wave velocity in the isotropic background model. To define the whole elastic tensor, we use the relation of these to the Love coefficients which can be found in first order as

$$A = \rho v_p^2 (1+a)^2,$$

$$L = N = \rho v_s^2,$$

$$F = \rho v_p^2 (1+a)(1+a+b),$$

$$C = \rho v_p^2 (1+a)(1+2a+2b+2c). \tag{46}$$

The good agreement between this simple ray theoretical perturbation method and the moveout of the body wave packets in Fig. 4 suggests that this is a feasible method to obtain full synthetic waveforms to study inner core anisotropic structures up to 2 Hz as shown here.

6 CONCLUSION AND OUTLOOK

This paper shows how the 2.5-D method by Nissen-Meyer *et al.* (2007a) is extended to include fully anisotropic structure. Two analytical arguments are provided to show that the terms in the expansion of the wave equation into a multipole series are still uncoupled: the first one was based on evaluation of the normal mode coupling matrix which has an intuitive interpretation in the global seismology context. The second one generalizes the idea to all linear equations that are invariant under rotation around an axis.

The resulting reduced equations are discretized using the spectral element method and the numerical implementation is benchmarked against a reference solution, showing excellent agreement both for high-frequency body waves and the low frequency normal mode spectra. Inner core anisotropy is suggested as one interesting application taking advantage of the specific parameter regime covered by this new version of *AxiSEM*.

Future work includes benchmarks for 2.5-D anisotropy and the application to more complex inner core anisotropy models as well as anisotropic D″ structures.

ACKNOWLEDGEMENTS

We thank the reviewers Heiner Igel and Yann Capdeville and the editor for the comments which helped to improve this manuscript. We gratefully acknowledge support from the European Commission (Marie Curie Actions, ITN QUEST, www.quest-itn.org). We thank David Al-Attar for valuable input on the theoretical section and providing his code *Yspec* as a reference. Heiner Igel's and Jeroen Tromp's critical comments led to the more rigorous considerations in Section 2. Lauren Waszek, Arwen Deuss and Jessica Irving gave valuable input for the inner core example. Data processing was done with extensive use of the *ObsPy* toolkit (Beyreuther *et al.* 2010; Megies *et al.* 2011). Computations where performed at the ETH central HPC cluster (Brutus), the Swiss National Supercomputing Center (CSCS) and the UK National Supercomputing Service (HECToR), whose support is gratefully acknowledged.

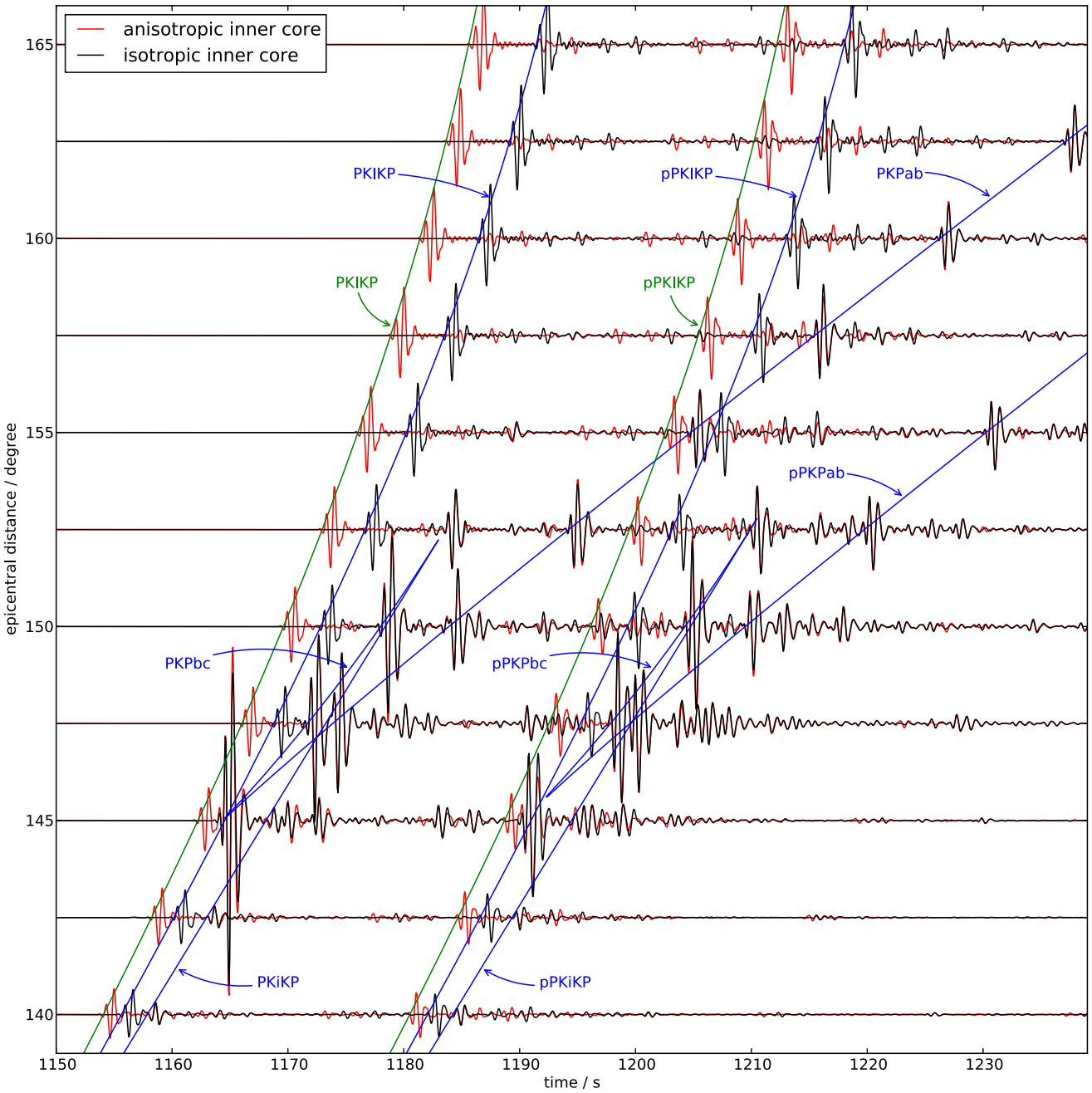

Figure 4. Vertical-displacement record section zoomed in to the inner-core phases for an explosive source bandpass filtered from 1 to 2 Hz. Normalization is global. Black traces for an isotropic PREM model, red traces for a PREM with anisotropic inner core (hexagonal symmetry, fast axis in north–south direction). Major ray theoretical arrivals in PREM are indicated with blue lines, *PKIKP* and *pPKIKP* for the anisotropic core with green lines computed according to eq. (45).

REFERENCES

Al-Attar, D. & Woodhouse, J.H., 2008. Calculation of seismic displacement fields in self-gravitating earth models—applications of minors vectors and symplectic structure, *Geophys. J. Int.,* **175**(3), 1176–1208.

Alkhalifah, T., 2000. An acoustic wave equation for anisotropic media, *Geophysics,* **65**(4), 1239–1250.

Alterman, Z. & Karal, F., 1968. Propagation of elastic waves in layered media by finite difference methods, *Bull. seism. Soc. Am.,* **58**(1), 367–398.

Auer, L., Boschi, L., Becker, T.W., Nissen-Meyer, T. & Giardini, D., 2013. Savani: a variable-resolution whole-mantle model of anisotropic shear-velocity variations based on multiple datasets, *J. geophys. Res.: Solid Earth,* **119**(4), 3006–3034.

Backus, G., 1962. Long-wave elastic anisotropy produced by horizontal layering, *J. geophys. Res.,* **67**(11), 4427–4440.

Bernardi, C., Dauge, M. & Maday, Y., 1999. *Spectral Methods for Axisymmetric Domains,* Gauthier-Villars.

Beyreuther, M., Barsch, R., Krischer, L., Megies, T., Behr, Y. & Wassermann, J., 2010. ObsPy: a python toolbox for seismology, *Seism. Res. Lett.,* **81**(3), 530–533.

Boué, P., Poli, P., Campillo, M., Pedersen, H., Briand, X. & Roux, P., 2013. Teleseismic correlations of ambient seismic noise for deep global imaging of the Earth, *Geophys. J. Int.,* **194**(2), 844–848.

Chaljub, E. & Tarantola, A., 1997. Sensitivity of SS precursors to topography on the uppermantle 660 km discontinuity, *Geophys. Res. Lett.,* **24**(21), 2613–2616.

Colombi, A., Nissen-Meyer, T., Boschi, L. & Giardini, D., 2012. Seismic waveform sensitivity to global boundary topography, *Geophys. J. Int.,* **191**(2), 832–848.

Colombi, A., Nissen-Meyer, T., Boschi, L. & Giardini, D., 2013. Seismic waveform inversion for core-mantle boundary topography, *Geophys. J. Int.,* **191**(2), 832–848.

Cottaar, S. & Romanowicz, B., 2013. Observations of changing anisotropy across the southern margin of the African LLSVP, *Geophys. J. Int.,* **195**(2), 1184–1195.

Creager, K., 1992. Anisotropy of the inner core from differential travel times of the phases PKP and PKIKP, *Nature,* **356,** 309–314.

Dahlen, F.A. & Tromp, J., 1998. *Theoretical Global Seismology,* Princeton University Press.

Dahlen, F.A., Hung, S.-H. & Nolet, G., 2000. Fréchet kernels for finite-frequency traveltimes – I. Theory, *Geophys. J. Int.,* **141,** 157–174.

de la Puente, J., Käser, M., Dumbser, M. & Igel, H., 2007. An arbitrary high-order discontinuous Galerkin method for elastic waves on unstructured meshes – IV. Anisotropy, *Geophys. J. Int.,* **169**(3), 1210–1228.

Deuss, A. & Woodhouse, J.H., 2001. Theoretical free-oscillation spectra: the importance of wide bandÂ coupling, *Geophys. J. Int.,* **146**(3), 833–842.

Deuss, A., Irving, J. C.E. & Woodhouse, J.H., 2010. Regional variation of inner core anisotropy from seismic normal mode observations., *Science (New York, N.Y.),* **328**(5981), 1018–20.

Dziewonski, A.M. & Anderson, D.L., 1981. Preliminary reference Earth model, *Phys. Earth planet. Inter.,* **25**(4), 297–356.

Fournier, A., Bunge, H.-P., Hollerbach, R. & Vilotte, J.-P., 2004. Application of the spectral-element method to the axisymmetric Navier-Stokes equation, *Geophys. J. Int.,* **156**(3), 682–700.

Friederich, W. & Dalkolmo, J., 1995. Complete synthetic seismograms for a spherically symmetric Earth by a numerical computation of the Green's function in the frequency domain, *Geophys. J. Int.,* **122**(2), 537–550.

Furumura, T., Kennett, B. L.N. & Furumura, M., 1998. Seismic wavefield calculation for laterally heterogeneous whole earth models using the pseudospectral method, *Geophys. J. Int.,* **135,** 845–860.

Guillot, L., Capdeville, Y. & Marigo, J.-J., 2010. 2-D non-periodic homogenization of the elastic wave equation: SH case, *Geophys. J. Int.,* **182**(3), 1438–1454.

Igel, H. & Weber, M., 1995. SH-wave propagation in the whole mantle using high-order finite differences, *Geophys. Res. Lett.,* **22**(6), 731–734.

Igel, H. & Weber, M., 1996. P-SV wave propagation in the Earth's mantle using finite differences: application to heterogeneous lowermost mantle structure, *Geophys. Res. Lett.,* **23**(5), 415–418.

Igel, H., Mora, P. & Riollet, B., 1995. Anisotropic wave propagation through finite-difference grids, *Geophysics,* **60**(4), 1203–1216.

Irving, J.C.E. & Deuss, A., 2011. Hemispherical structure in inner core velocity anisotropy, *J. geophys. Res.,* **116**(B4), doi:10.1029/2010JB007942.

Irving, J.C.E., Deuss, A. & Andrews, J., 2008. Wide-band coupling of Earth's normal modes due to anisotropic inner core structure, *Geophys. J. Int.,* **174**(3), 919–929.

Irving, J. C.E., Deuss, A. & Woodhouse, J.H., 2009. Normal mode coupling due to hemispherical anisotropic structure in Earth's inner core, *Geophys. J. Int.,* **178**(2), 962–975.

Jahnke, G., Thorne, M.S., Cochard, A. & Igel, H., 2008. Global SH-wave propagation using a parallel axisymmetric spherical finite-difference scheme: application to whole mantle scattering, *Geophys. J. Int.,* **173**(3), 815–826.

Kennett, B. L.N., Engdahl, E.R. & Buland, R., 1995. Constraints on seismic velocities in the Earth from traveltimes, *Geophys. J. Int.,* **122,** 108–124.

Komatitsch, D., Barnes, C. & Tromp, J., 2000. Simulation of anisotropic wave propagation based upon a spectral element method, *Geophysics,* **65**(4), 1251–1260.

Kristekova, M., Kristek, J. & Moczo, P., 2009. Time-frequency misfit and goodness-of-fit criteria for quantitative comparison of time signals, *Geophys. J. Int.,* **178**(2), 813–825.

Kustowski, B., Ekström, G. & Dziewoski, A.M., 2008. Anisotropic shear-wave velocity structure of the Earth's mantle: A global model, *J. geophys. Res.,* **113**(B6), B06306, doi:10.1029/2007JB005169.

Long, M.D., 2009. Complex anisotropy in D″ beneath the eastern Pacific from SKS-SKKS splitting discrepancies, *Earth planet. Sci. Lett.,* **283** (1–4), 181–189.

Long, M.D. & Becker, T.W., 2010. Mantle dynamics and seismic anisotropy, *Earth planet. Sci. Lett.,* **297**(3–4), 341–354.

Megies, T., Beyreuther, M., Barsch, R., Krischer, L. & Wassermann, J., 2011. ObsPy—what can it do for data centers and observatories?, *Ann. Geophys.,* **54**(1), doi:10.4401/ag-4838.

Moczo, P., Robertsson, J. & Eisner, L., 2007. The finite-difference time-domain method for modeling of seismic wave propagation, *Adv. Geophys.,* **48,** 421–516.

Morelli, A., Dziewoski, A.M. & Woodhouse, J.H., 1986. Anisotropy of the inner core inferred from PKIKP travel times, *Geophys. Res. Lett.,* **13**(13), 1545–1548.

Nissen-Meyer, T., Dahlen, F.A. & Fournier, A., 2007a. Spherical-earth Fréchet sensitivity kernels, *Geophys. J. Int.,* **168**(3), 1051–1066.

Nissen-Meyer, T., Fournier, A. & Dahlen, F.A., 2007b. A two-dimensional spectral-element method for computing spherical-earth seismograms – I. Moment-tensor source, *Geophys. J. Int.,* **168**(3), 1067–1092.

Nissen-Meyer, T., Fournier, A. & Dahlen, F.A., 2008. A 2-D spectral-element method for computing spherical-Earth seismograms – II. Waves in solid-fluid media, *Geophys. J. Int.,* **174**(3), 873–888.

Nissen-Meyer, T., van Driel, M., Stähler, S.C., Hosseini, K., Hempel, S., Auer, L., Colombi, A. & Fournier, A., 2014. AxiSEM: broadband 3-D seismic wavefields in axisymmetric media, *Solid Earth,* **5**(1), 425–445.

Nowacki, A., Wookey, J. & Kendall, J.-M., 2011. New advances in using seismic anisotropy, mineral physics and geodynamics to understand deformation in the lowermost mantle, *J. Geodyn.,* **52**(3–4), 205–228.

Panning, M. & Romanowicz, B., 2004. Inferences on flow at the base of Earth's mantle based on seismic anisotropy, *Science,* **303**(5656), 351–353.

Panning, M.P., Lekić, V. & Romanowicz, B.A., 2010. Importance of crustal corrections in the development of a new global model of radial anisotropy, *J. geophys. Res.,* **115**(B12), B12325, doi:10.1029/2010JB007520.

Phinney, R.A. & Burridge, R., 1973. Representation of the elastic—gravitational excitation of a spherical Earth model, *Geophys. J. R. astr. Soc.,* **34,** 451–487.

Stähler, S.C., Sigloch, K. & Nissen-Meyer, T., 2012. Triplicated P-wave measurements for waveform tomography of the mantle transition zone, *Solid Earth,* **3**(2), 339–354.

Takenaka, H., Tanaka, H., Okamoto, T. & Kennett, B.L.N., 2003. Quasi-cylindrical 2.5D wave modeling for large-scale seismic surveys, *Geophys. Res. Lett.,* **30**(21), doi:10.1029/2003GL018068.

Thomas, C., Igel, H., Weber, M. & Scherbaum, F., 2000. Acoustic simulation of P-wave propagation in a heterogeneous spherical Earth: numerical method and application to precursor waves to PKPdf, *Geophys. J. Int.,* **141,** 307–320.

Toyokuni, G. & Takenaka, H., 2006. FDM computation of seismic wavefield for an axisymmetric Earth with a moment tensor point source, *Earth Planets Space,* **58,** e29–e32.

Toyokuni, G. & Takenaka, H., 2012. Accurate and efficient modeling of global seismic wave propagation for an attenuative Earth model including the center, *Phys. Earth planet. Inter.,* **200–201,** 45–55.

Toyokuni, G., Takenaka, H., Wang, Y. & Kennett, B.L.N., 2005. Quasi-spherical approach for seismic wave modeling in a 2-D slice of a global Earth model with lateral heterogeneity, *Geophys. Res. Lett.,* **32,** doi:10.1029/2004GL022180.

Walker, A.M., Forte, A.M., Wookey, J., Nowacki, A. & Kendall, J.-M., 2011. Elastic anisotropy of D″ predicted from global models of mantle flow, *Geochem. Geophys. Geosyst.,* **12**(10), doi:10.1029/2011GC003732.

Wang, N., Montagner, J.-P., Fichtner, A. & Capdeville, Y., 2013. Intrinsic versus extrinsic seismic anisotropy: the radial anisotropy in reference Earth models, *Geophys. Res. Lett.,* **40**(16), 4284–4288.

Waszek, L. & Deuss, A., 2011. Distinct layering in the hemispherical seismic velocity structure of Earth's upper inner core, *J. geophys. Res.,* **116,** B12313, doi:10.1029/2011JB008650.

Waszek, L., Irving, J. & Deuss, A., 2011. Reconciling the hemispherical structure of Earth's inner core with its super-rotation, *Nat. Geosci.,* **4**(4), 264–267.

Woodhouse, J.H., 1983. The joint inversion of seismic waveforms for lateral variations in Earth structure and earthquake source parameters, in *Proceedings of the Enrico Fermi International School of Physics,* Vol. 85, pp. 366–397, eds Kanamori, H. & Boschi, E., North-Holland, Amsterdam.

Woodhouse, J.H. & Dahlen, F.A., 1978. The effect of a general aspherical perturbation on the free oscillations of the Earth, *Geophys. J. R. astr. Soc.,* **53,** 335–354.

Woodhouse, J.H. & Deuss, A., 2007. Theory and observations – Earth's free oscillations, in *Treatise on Geophysics,* Vol. 1, pp. 31–65, Elsevier, Amsterdam.

APPENDIX A: DIPOLE AND QUADRUPOLE STIFFNESS TERMS

This section contains the results for the weak form of the stiffness term for dipole and quadrupole sources, equivalent to the results presented in Section 3.1 for the monopole source and Nissen-Meyer *et al.* (2007a, Section 4.6–7) for the isotropic case.

A1 Dipole ($m = 1$)

For the dipole source, we define

$$u_\pm = \frac{1}{2}(u_s \pm u_\varphi) \quad \Rightarrow \quad u_s = u_+ + u_-, \quad u_\varphi = u_+ - u_- \tag{A1}$$

as this facilitates easier implementation of the axial boundary conditions (compare Nissen-Meyer *et al.* 2007a, Section 4.8). The stiffness terms integrated over φ then read

$$\begin{aligned}
&\frac{1}{\pi}\int_0^{2\pi} \nabla\mathbf{w} : (\boldsymbol{c} : \nabla\mathbf{u})\, \mathrm{d}\varphi \\
&= \partial_s w_+ \Big(((C_{11}+C_{66})\partial_s u_+ + (C_{11}-C_{66})\partial_s u_- + C_{15}\partial_s u_z \\
&\qquad + (C_{15}+C_{46})\partial_z u_+ + (C_{15}-C_{46})\partial_z u_- + C_{13}\partial_z u_z \\
&\qquad + \frac{1}{s}(2(C_{12}+C_{66})u_- + C_{46}u_z)\Big) \\
&+ \partial_z w_+ \Big(((C_{15}+C_{46})\partial_s u_+ + (C_{15}-C_{46})\partial_s u_- + C_{55}\partial_s u_z \\
&\qquad + (C_{55}+C_{44})\partial_z u_+ + (C_{55}-C_{44})\partial_z u_- + C_{35}\partial_z u_z \\
&\qquad + \frac{1}{s}(2(C_{46}+C_{25})u_- + C_{44}u_z)\Big) \\
&+ \partial_s w_- \Big(((C_{11}-C_{66})\partial_s u_+ + (C_{11}+C_{66})\partial_s u_- + C_{15}\partial_s u_z \\
&\qquad + (C_{15}-C_{46})\partial_z u_+ + (C_{15}+C_{46})\partial_z u_- + C_{13}\partial_z u_z \\
&\qquad + \frac{1}{s}(2(C_{12}-C_{66})u_- - C_{46}u_z)\Big) \\
&+ \partial_z w_- \Big(((C_{15}-C_{46})\partial_s u_+ + (C_{15}+C_{46})\partial_s u_- + C_{55}\partial_s u_z \\
&\qquad + (C_{55}-C_{44})\partial_z u_+ + (C_{55}+C_{44})\partial_z u_- + C_{35}\partial_z u_z \\
&\qquad + \frac{1}{s}(2(-C_{46}+C_{25})u_- - C_{44}u_z)\Big) \\
&+ \frac{2}{s} w_- \Big(((C_{12}+C_{66})\partial_s u_+ + (C_{12}-C_{66})\partial_s u_- + C_{25}\partial_s u_z \\
&\qquad + (C_{25}+C_{46})\partial_z u_+ + (C_{25}-C_{46})\partial_z u_- + C_{23}\partial_z u_z \\
&\qquad + \frac{1}{s}(2(C_{22}+C_{66})u_- + C_{46}u_z)\Big) \\
&+ \partial_s w_z \Big(C_{15}\partial_s u_+ + C_{15}\partial_s u_- + C_{55}\partial_s u_z \\
&\qquad + C_{55}\partial_z u_+ + C_{55}\partial_z u_- + C_{35}\partial_z u_z + \frac{2}{s}C_{25}u_-\Big) \\
&+ \partial_z w_z \Big(C_{13}\partial_s u_+ + C_{13}\partial_s u_- + C_{35}\partial_s u_z \\
&\qquad + C_{35}\partial_z u_+ + C_{35}\partial_z u_- + C_{33}\partial_z u_z + \frac{2}{s}C_{23}u_-\Big) \\
&+ \frac{w_z}{s}\Big(C_{46}\partial_s u_+ - C_{46}\partial_s u_- + C_{44}\partial_z u_+ \\
&\qquad - C_{44}\partial_z u_- + \frac{2}{s}C_{46}u_-\Big).
\end{aligned} \tag{A2}$$

A2 Quadrupole ($m = 2$)

In the quadrupole case we remain with the same basis as for the monopole (u_s, u_φ, u_z) and find the stiffness terms integrated over φ as

$$\begin{aligned}
&\frac{1}{2\pi}\int_0^{2\pi} \nabla\mathbf{w} : (\boldsymbol{c} : \nabla\mathbf{u})\, \mathrm{d}\varphi \\
&= \partial_s w_s \Big(C_{11}\partial_s u_s + C_{15}\partial_z u_s + C_{15}\partial_s u_z + C_{13}\partial_z u_z \\
&\qquad + \frac{1}{s}(C_{12}u_s - 2C_{12}u_\varphi)\Big) \\
&+ \partial_z w_s \Big(C_{15}\partial_s u_s + C_{55}\partial_z u_s + C_{55}\partial_s u_z + C_{35}\partial_z u_z \\
&\qquad + \frac{1}{s}(C_{25}u_s - 2C_{25}u_\varphi)\Big) \\
&+ \frac{1}{s} w_s \Big(C_{12}\partial_s u_s + 2C_{66}\partial_s u_\varphi + C_{25}\partial_s u_z \\
&\qquad + C_{25}\partial_z u_s + 2C_{46}\partial_z u_\varphi + C_{23}\partial_z u_z \\
&\qquad + \frac{1}{s}((C_{22}+4C_{66})u_s - 2(C_{22}+C_{66})u_\varphi + 4C_{46}u_z)\Big) \\
&+ \partial_s w_\varphi \Big(C_{66}\partial_s u_\varphi + C_{46}\partial_z u_\varphi + \frac{1}{s}(2C_{66}u_s \\
&\qquad - C_{66}u_\varphi + 2C_{46}u_z)\Big) \\
&+ \partial_z w_\varphi \Big(C_{46}\partial_s u_\varphi + C_{44}\partial_z u_\varphi + \frac{1}{s}(2C_{46}u_s \\
&\qquad - C_{46}u_\varphi + 2C_{44}u_z)\Big) \\
&+ \frac{1}{s} w_\varphi \Big(-2C_{12}\partial_s u_s - 2C_{25}\partial_s u_z - C_{66}\partial_s u_\varphi \\
&\qquad - 2C_{23}\partial_z u_z - 2C_{25}\partial_z u_s - C_{46}\partial_z u_\varphi \\
&\qquad + \frac{1}{s}(-2C_{22}u_s + 4C_{22}u_\varphi + C_{66}u_\varphi \\
&\qquad\quad - 2C_{66}u_s - 2C_{46}u_z)\Big) \\
&+ \partial_s w_z \Big(C_{15}\partial_s u_s + C_{55}\partial_z u_s + C_{55}\partial_s u_z + C_{35}\partial_z u_z \\
&\qquad + \frac{1}{s}(C_{25}u_s - 2C_{25}u_\varphi)\Big) \\
&+ \partial_z w_z \Big(C_{13}\partial_s u_s + C_{35}\partial_z u_s + C_{35}\partial_s u_z + C_{33}\partial_z u_z \\
&\qquad + \frac{1}{s}(C_{23}u_s - 2C_{23}u_\varphi)\Big)
\end{aligned}$$

$$+\frac{2}{s}w_z\Big(C_{46}\partial_s u_\varphi + C_{44}\partial_z u_\varphi + \frac{1}{s}(2C_{46}u_s - C_{46}u_\varphi + 2C_{44}u_z)\Big). \tag{A3}$$

APPENDIX B: DIPOLE AND QUADRUPOLE DISCRETIZATION OF THE STIFFNESS TERMS

These stiffness terms are then discretized in the SEM using the notation defined in Section 3.2.

B1 Dipole

For the dipole, we define $\mathbf{E}^{(k)}_{\beta\alpha}$ for the leading order terms as

$$\begin{aligned}
\mathbf{E}^{(k)}_{++} &= {}_{(C_{11}+C_{66})}\mathbf{G}^{ss}_k + {}_{(C_{15}+C_{46})}\mathbf{G}^{sz}_k \\
&\quad + {}_{(C_{15}+C_{46})}\mathbf{G}^{zs}_k + {}_{(C_{55}+C_{44})}\mathbf{G}^{zz}_k \\
\mathbf{E}^{(k)}_{+-} &= {}_{(C_{11}-C_{66})}\mathbf{G}^{ss}_k + {}_{(C_{15}-C_{46})}\mathbf{G}^{sz}_k \\
&\quad + {}_{(C_{15}-C_{46})}\mathbf{G}^{zs}_k + {}_{(C_{55}-C_{44})}\mathbf{G}^{zz}_k \\
\mathbf{E}^{(k)}_{+z} &= {}_{C_{15}}\mathbf{G}^{ss}_k + {}_{C_{13}}\mathbf{G}^{sz}_k + {}_{C_{55}}\mathbf{G}^{zs}_k + {}_{C_{35}}\mathbf{G}^{zz}_k
\end{aligned} \tag{B1}$$

$$\mathbf{E}^{(k)}_{-+} = \mathbf{E}^{(k)}_{+-} \qquad \mathbf{E}^{(k)}_{--} = \mathbf{E}^{(k)}_{++} \qquad \mathbf{E}^{(k)}_{-z} = \mathbf{E}^{(k)}_{+z} \tag{B2}$$

$$\begin{aligned}
\mathbf{E}^{(k)}_{z+} &= {}_{C_{15}}\mathbf{G}^{ss}_k + {}_{C_{55}}\mathbf{G}^{sz}_k + {}_{C_{13}}\mathbf{G}^{zs}_k + {}_{C_{35}}\mathbf{G}^{zz}_k \\
\mathbf{E}^{(k)}_{z-} &= \mathbf{E}^{(k)}_{z+} \\
\mathbf{E}^{(k)}_{zz} &= {}_{C_{55}}\mathbf{G}^{ss}_k + {}_{C_{35}}\mathbf{G}^{sz}_k + {}_{C_{35}}\mathbf{G}^{zs}_k + {}_{C_{33}}\mathbf{G}^{zz}_k .
\end{aligned} \tag{B3}$$

The leading order terms then are

$$(\mathbf{Ku})^{\partial\partial}_\beta = \sum_{\alpha\in\{+,-,z\}} (\mathbf{Ku})^{\partial\partial}_{\beta\alpha}, \tag{B4}$$

with $(\mathbf{Ku})^{\partial\partial}_{\beta\alpha}$ from eq. (40). For the lower order and axial terms we define

$$\begin{aligned}
\mathbf{M}_1 &= {}_{(2C_{12}+2C_{66})}\mathbf{B}_{z_\eta} + {}_{(2C_{25}+2C_{46})}\mathbf{B}_{s_\eta} \\
\mathbf{M}_2 &= {}_{(2C_{12}+2C_{66})}\mathbf{B}_{z_\xi} + {}_{(2C_{25}+2C_{46})}\mathbf{B}_{s_\xi} \\
\mathbf{M}_3 &= {}_{C_{46}}\mathbf{B}_{z_\eta} + {}_{C_{44}}\mathbf{B}_{s_\eta} \\
\mathbf{M}_4 &= {}_{C_{46}}\mathbf{B}_{z_\xi} + {}_{C_{44}}\mathbf{B}_{s_\xi} \\
\mathbf{M}_5 &= {}_{(2C_{12}-2C_{66})}\mathbf{B}_{z_\eta} + {}_{(2C_{25}-2C_{46})}\mathbf{B}_{s_\eta} \\
\mathbf{M}_6 &= {}_{(2C_{12}-2C_{66})}\mathbf{B}_{z_\xi} + {}_{(2C_{25}-2C_{46})}\mathbf{B}_{s_\xi} \\
\mathbf{M}_7 &= {}_{2C_{25}}\mathbf{B}_{z_\eta} + {}_{2C_{23}}\mathbf{B}_{s_\eta} \\
\mathbf{M}_8 &= {}_{2C_{25}}\mathbf{B}_{z_\xi} + {}_{2C_{23}}\mathbf{B}_{s_\xi},
\end{aligned} \tag{B5}$$

$$\begin{aligned}
\mathbf{M}_{w1} &= {}_{(4C_{22}+4C_{66})}\mathbf{A} \qquad \mathbf{M}_{w2} = {}_{2C_{46}}\mathbf{A} \\
\mathbf{M}_{w3} &= {}_{C_{44}}\mathbf{A}
\end{aligned} \tag{B6}$$

and

$$\begin{aligned}
\mathbf{M}^0_{w1} &= {}_{(2C_{12}+2C_{66})}\mathbf{A}^0 \qquad \mathbf{M}^0_{w2} = {}_{(2C_{12}+2C_{66})}\mathbf{B}^0_{z_\xi} \\
\mathbf{M}^0_{w3} &= {}_{C_{46}}\mathbf{A}^0 \qquad \mathbf{M}^0_{w4} = {}_{C_{46}}\mathbf{B}^0_{z_\xi} \\
\mathbf{M}^0_{w5} &= {}_{(2C_{25}+2C_{46})}\mathbf{A}^0 \qquad \mathbf{M}^0_{w6} = {}_{(2C_{25}+2C_{46})}\mathbf{B}^0_{s_\xi} \\
\mathbf{M}^0_{w7} &= {}_{C_{44}}\mathbf{A}^0 \qquad \mathbf{M}^0_{w8} = {}_{C_{44}}\mathbf{B}^0_{s_\xi} \\
\mathbf{M}^0_{w9} &= {}_{(4C_{12}+4C_{22})}\mathbf{A}^0 \qquad \mathbf{M}^0_{w10} = {}_{(2C_{25}+C_{46})}\mathbf{A}^0.
\end{aligned} \tag{B7}$$

The lower order terms can then be written as

$$\begin{aligned}
(\mathbf{Ku})^\partial_+ &= \mathbf{D}_\xi \otimes \big[\mathbf{M}_1 \odot \mathbf{u}_- + \mathbf{M}_3 \odot \mathbf{u}_z\big] \\
&\quad + \big[\mathbf{M}_2 \odot \mathbf{u}_- + \mathbf{M}_4 \odot \mathbf{u}_z\big] \otimes \mathbf{D}^{\mathrm{T}}_\eta \\
&\quad + \delta_{e\bar{e}}\Big\{\mathbf{D}^0_\xi\Big[\mathbf{M}^0_{w1} \odot \Big(\big(\mathbf{D}^0_\xi\big)^{\mathrm{T}} \otimes \mathbf{u}_-\Big) \\
&\qquad + \mathbf{M}^0_{w3} \odot \Big(\big(\mathbf{D}^0_\xi\big)^{\mathrm{T}} \otimes \mathbf{u}_z\Big)\Big] \\
&\qquad + \Big[\big(\mathbf{M}^0_{w2} + \mathbf{M}^0_{w6}\big) \odot \Big(\big(\mathbf{D}^0_\xi\big)^{\mathrm{T}} \otimes \mathbf{u}_-\Big) \\
&\qquad + \big(\mathbf{M}^0_{w4} + \mathbf{M}^0_{w8}\big) \odot \Big(\big(\mathbf{D}^0_\xi\big)^{\mathrm{T}} \otimes \mathbf{u}_z\Big)\Big] \otimes \mathbf{D}^{\mathrm{T}}_\eta\Big\},
\end{aligned} \tag{B8}$$

$$\begin{aligned}
(\mathbf{Ku})^\partial_- &= \mathbf{M}_1 \odot \big(\mathbf{D}^{\mathrm{T}}_\xi \otimes \mathbf{u}_+\big) + \mathbf{M}_2 \odot \big(\mathbf{u}_+ \otimes \mathbf{D}_\eta\big) \\
&\quad + \mathbf{M}_5 \odot \big(\mathbf{D}^{\mathrm{T}}_\xi \otimes \mathbf{u}_-\big) + \mathbf{M}_6 \odot \big(\mathbf{u}_- \otimes \mathbf{D}_\eta\big) \\
&\quad + \mathbf{M}_7 \odot \big(\mathbf{D}^{\mathrm{T}}_\xi \otimes \mathbf{u}_z\big) + \mathbf{M}_8 \odot \big(\mathbf{u}_z \otimes \mathbf{D}_\eta\big) \\
&\quad + \mathbf{D}_\xi \otimes \big[\mathbf{M}_5 \odot \mathbf{u}_- - \mathbf{M}_3 \odot \mathbf{u}_z\big] \\
&\quad + \big[\mathbf{M}_6 \odot \mathbf{u}_- - \mathbf{M}_4 \odot \mathbf{u}_z\big] \otimes \mathbf{D}^{\mathrm{T}}_\eta \\
&\quad + \mathbf{M}_{w1} \odot \mathbf{u}_- + \mathbf{M}_{w2} \odot \mathbf{u}_z \\
&\quad + \delta_{e\bar{e}}\mathbf{D}^0_\xi\Big[\mathbf{M}^0_{w1} \odot \Big(\big(\mathbf{D}^0_\xi\big)^{\mathrm{T}} \otimes \mathbf{u}_+\Big) \\
&\qquad + \mathbf{M}^0_{w6} \odot \big(\mathbf{u}^0_+ \otimes \mathbf{D}_\eta\big) \\
&\qquad + \mathbf{M}^0_{w9} \odot \Big(\big(\mathbf{D}^0_\xi\big)^{\mathrm{T}} \otimes \mathbf{u}_-\Big) \\
&\qquad + \mathbf{M}^0_{w2} \odot \big(\mathbf{u}^0_- \otimes \mathbf{D}_\eta\big) \\
&\qquad + \mathbf{M}^0_{w10} \odot \Big(\big(\mathbf{D}^0_\xi\big)^{\mathrm{T}} \otimes \mathbf{u}_z\Big)\Big]
\end{aligned} \tag{B9}$$

and

$$\begin{aligned}
(\mathbf{Ku})^\partial_z &= \mathbf{M}_3 \odot \big(\mathbf{D}^{\mathrm{T}}_\xi \otimes (\mathbf{u}_+ - \mathbf{u}_-)\big) \\
&\quad + \mathbf{M}_4 \odot \big((\mathbf{u}_+ - \mathbf{u}_-) \otimes \mathbf{D}_\eta\big) \\
&\quad + \mathbf{D}_\xi \otimes \big[\mathbf{M}_7 \odot \mathbf{u}_-\big] + \big[\mathbf{M}_8 \odot \mathbf{u}_-\big] \otimes \mathbf{D}^{\mathrm{T}}_\eta \\
&\quad + \mathbf{M}_{w2} \odot \mathbf{u}_- + \mathbf{M}_{w3} \odot \mathbf{u}_z \\
&\quad + \delta_{e\bar{e}}\mathbf{D}^0_\xi\Big[\mathbf{M}^0_{w3} \odot \Big(\big(\mathbf{D}^0_\xi\big)^{\mathrm{T}} \otimes \mathbf{u}_+\Big) \\
&\qquad + \big(\mathbf{M}^0_{w4} + \mathbf{M}^0_{w8}\big) \odot \big(\mathbf{u}^0_+ \otimes \mathbf{D}_\eta\big) \\
&\qquad + \mathbf{M}^0_{w10} \odot \Big(\big(\mathbf{D}^0_\xi\big)^{\mathrm{T}} \otimes \mathbf{u}_-\Big) \\
&\qquad + \mathbf{M}^0_{w7} \odot \Big(\big(\mathbf{D}^0_\xi\big)^{\mathrm{T}} \otimes \mathbf{u}_z\Big)\Big].
\end{aligned} \tag{B10}$$

B2 Quadrupole

For the quadrupole source, we define additionally to the definitions from the monopole, eq. (41)

$$\begin{aligned}
\mathbf{E}^{(k)}_{\varphi\varphi} &= {}_{C_{66}}\mathbf{G}^{ss}_k + {}_{C_{46}}\mathbf{G}^{sz}_k + {}_{C_{46}}\mathbf{G}^{zs}_k + {}_{C_{44}}\mathbf{G}^{zz}_k \\
\mathbf{E}^{(k)}_{\varphi s} &= 0 \qquad \mathbf{E}^{(k)}_{\varphi z} = 0 \qquad \mathbf{E}^{(k)}_{s\varphi} = 0 \qquad \mathbf{E}^{(k)}_{z\varphi} = 0.
\end{aligned} \tag{B11}$$

The leading order terms then are

$$(\mathbf{Ku})^{\partial\partial}_\beta = \sum_{\alpha\in\{s,\varphi,z\}} (\mathbf{Ku})^{\partial\partial}_{\beta\alpha}. \tag{B12}$$

Additionally to $\mathbf{M}_1, \mathbf{M}_2, \mathbf{M}_3, \mathbf{M}_4$ as in the monopole case, eq. (42) we define:

$$\begin{aligned}
\mathbf{M}_5 &= {}_{C_{66}}\mathbf{B}_{z_\eta} + {}_{C_{46}}\mathbf{B}_{s_\eta} \qquad & \mathbf{M}_6 &= {}_{C_{66}}\mathbf{B}_{z_\xi} + {}_{C_{46}}\mathbf{B}_{s_\xi} \\
\mathbf{M}_7 &= {}_{C_{46}}\mathbf{B}_{z_\eta} + {}_{C_{44}}\mathbf{B}_{s_\eta} \qquad & \mathbf{M}_8 &= {}_{C_{46}}\mathbf{B}_{z_\xi} + {}_{C_{44}}\mathbf{B}_{s_\xi}
\end{aligned} \tag{B13}$$

and partly redefine:

$$\begin{aligned}
\mathbf{M}_{w1} &= {}_{(C_{22}+4C_{66})}\mathbf{A} \qquad & \mathbf{M}_{w2} &= {}_{-2(C_{22}+C_{66})}\mathbf{A} \\
\mathbf{M}_{w3} &= {}_{2C_{46}}\mathbf{A} \qquad & \mathbf{M}_{w4} &= {}_{(4C_{22}+C_{66})}\mathbf{A} \\
\mathbf{M}_{w5} &= {}_{4C_{44}}\mathbf{A} \\
\mathbf{M}^0_{w1} &= {}_{(2C_{12}+C_{22}+4C_{66})}\mathbf{A}^0 \qquad & \mathbf{M}^0_{w2} &= {}_{-2(C_{12}+C_{22})}\mathbf{A}^0 \\
\mathbf{M}^0_{w3} &= {}_{(C_{25}+4C_{46})}\mathbf{A}^0 \qquad & \mathbf{M}^0_{w4} &= {}_{(4C_{22}-C_{66})}\mathbf{A}^0 \\
\mathbf{M}^0_{w5} &= {}_{-2C_{25}}\mathbf{A}^0 \qquad & \mathbf{M}^0_{w6} &= {}_{4C_{44}}\mathbf{A}^0.
\end{aligned} \tag{B14}$$

The lower order terms can then be written as

$$\begin{aligned}
(\mathbf{Ku})^\partial_s = {}& \mathbf{M}_1 \odot \left(\mathbf{D}^{\mathrm{T}}_\xi \otimes \mathbf{u}_s\right) + \mathbf{M}_2 \odot \left(\mathbf{u}_s \otimes \mathbf{D}_\eta\right) \\
&+ \mathbf{M}_3 \odot \left(\mathbf{D}^{\mathrm{T}}_\xi \otimes \mathbf{u}_z\right) + \mathbf{M}_4 \odot \left(\mathbf{u}_z \otimes \mathbf{D}_\eta\right) \\
&+ 2 \cdot \mathbf{M}_5 \odot \left(\mathbf{D}^{\mathrm{T}}_\xi \otimes \mathbf{u}_\varphi\right) + 2 \cdot \mathbf{M}_6 \odot \left(\mathbf{u}_\varphi \otimes \mathbf{D}_\eta\right) \\
&+ \mathbf{D}_\xi \otimes \left(\mathbf{M}_1 \odot (\mathbf{u}_s - 2\mathbf{u}_\varphi)\right) + \left(\mathbf{M}_2 \odot (\mathbf{u}_s - 2\mathbf{u}_\varphi)\right) \otimes \mathbf{D}^{\mathrm{T}}_\eta \\
&+ \mathbf{M}_{w1} \odot \mathbf{u}_s + \mathbf{M}_{w2} \odot \mathbf{u}_\varphi + 2\mathbf{M}_{w3} \odot \mathbf{u}_z \\
&+ \delta_{e\bar{e}} \cdot \mathbf{D}^0_\xi \Big[\mathbf{M}^0_{w1} \odot \left(\left(\mathbf{D}^0_\xi\right)^{\mathrm{T}} \otimes \mathbf{u}_s\right) \\
&\qquad + \mathbf{M}^0_{w2} \odot \left(\left(\mathbf{D}^0_\xi\right)^{\mathrm{T}} \otimes \mathbf{u}_\varphi\right) \\
&\qquad + \mathbf{M}^0_{w3} \odot \left(\left(\mathbf{D}^0_\xi\right)^{\mathrm{T}} \otimes \mathbf{u}_z\right) \Big]
\end{aligned} \tag{B15}$$

$$\begin{aligned}
(\mathbf{Ku})^\partial_\varphi = {}& -2 \cdot \mathbf{M}_1 \odot \left(\mathbf{D}^{\mathrm{T}}_\xi \otimes \mathbf{u}_s\right) - 2 \cdot \mathbf{M}_2 \odot \left(\mathbf{u}_s \otimes \mathbf{D}_\eta\right) \\
&- 2 \cdot \mathbf{M}_3 \odot \left(\mathbf{D}^{\mathrm{T}}_\xi \otimes \mathbf{u}_z\right) - 2 \cdot \mathbf{M}_4 \odot \left(\mathbf{u}_z \otimes \mathbf{D}_\eta\right) \\
&- \mathbf{M}_5 \odot \left(\mathbf{D}^{\mathrm{T}}_\xi \otimes \mathbf{u}_\varphi\right) - \mathbf{M}_6 \odot \left(\mathbf{u}_\varphi \otimes \mathbf{D}_\eta\right) \\
&+ \mathbf{D}_\xi \otimes \left[\mathbf{M}_5 \odot (2\mathbf{u}_s - \mathbf{u}_\varphi) + 2 \cdot \mathbf{M}_7 \odot \mathbf{u}_z\right] \\
&+ \left[\mathbf{M}_6 \odot (2\mathbf{u}_s - \mathbf{u}_\varphi) + 2 \cdot \mathbf{M}_8 \odot \mathbf{u}_z\right] \otimes \mathbf{D}^{\mathrm{T}}_\eta \\
&+ \mathbf{M}_{w2} \odot \mathbf{u}_s + \mathbf{M}_{w4} \odot \mathbf{u}_\varphi - \mathbf{M}_{w3} \odot \mathbf{u}_z \\
&+ \delta_{e\bar{e}} \cdot \mathbf{D}^0_\xi \Big[\mathbf{M}^0_{w2} \odot \left(\left(\mathbf{D}^0_\xi\right)^{\mathrm{T}} \otimes \mathbf{u}_s\right) \\
&\qquad + \mathbf{M}^0_{w4} \odot \left(\left(\mathbf{D}^0_\xi\right)^{\mathrm{T}} \otimes \mathbf{u}_\varphi\right) \\
&\qquad + \mathbf{M}^0_{w5} \odot \left(\left(\mathbf{D}^0_\xi\right)^{\mathrm{T}} \otimes \mathbf{u}_z\right) \Big]
\end{aligned} \tag{B16}$$

$$\begin{aligned}
(\mathbf{Ku})^\partial_z = {}& 2 \cdot \mathbf{M}_7 \odot \left(\mathbf{D}^{\mathrm{T}}_\xi \otimes \mathbf{u}_\varphi\right) + 2 \cdot \mathbf{M}_8 \odot \left(\mathbf{u}_\varphi \otimes \mathbf{D}_\eta\right) \\
&+ \mathbf{D}_\xi \otimes \left(\mathbf{M}_3 \odot (\mathbf{u}_s - 2\mathbf{u}_\varphi)\right) \\
&+ \left(\mathbf{M}_4 \odot (\mathbf{u}_s - 2\mathbf{u}_\varphi)\right) \otimes \mathbf{D}^{\mathrm{T}}_\eta \\
&+ \mathbf{M}_{w3} \odot (2\mathbf{u}_s - \mathbf{u}_\varphi) + \mathbf{M}_{w5} \odot \mathbf{u}_z \\
&+ \delta_{e\bar{e}} \cdot \mathbf{D}^0_\xi \Big[\mathbf{M}^0_{w3} \odot \left(\left(\mathbf{D}^0_\xi\right)^{\mathrm{T}} \otimes \mathbf{u}_s\right) \\
&\qquad + \mathbf{M}^0_{w5} \odot \left(\left(\mathbf{D}^0_\xi\right)^{\mathrm{T}} \otimes \mathbf{u}_\varphi\right) \\
&\qquad + \mathbf{M}^0_{w6} \odot \left(\left(\mathbf{D}^0_\xi\right)^{\mathrm{T}} \otimes \mathbf{u}_z\right) \Big].
\end{aligned} \tag{B17}$$